Thesis for the Degree of Master of Science

Emission Mechanism of Blazar OJ 287

Hyunjoo Goh

Department of Astronomy and Space Science
Graduate School
Kyung Hee University
Seoul, Korea

August, 2009

Emission Mechanism of Blazar OJ 287

Hyunjoo Goh

Department of Astronomy and Space Science
Graduate School
Kyung Hee University
Seoul, Korea

August, 2009

Emission Mechanism of Blazar OJ 287

by

Hyunjoo Goh

Advised by

Dr. Soojong Pak

Submitted to the Department of Astronomy and Space Science
and the Faculty of the Graduate School of Kyung Hee University
in partial fulfillment of the requirements for
degree of Master of Science

Dissertation Committee:

____
Dr. Soojong Pak

____
Dr. Minhwan Jang

____
Dr. Bong Won Sohn

Abstract

We present the result of optical monitoring of the blazar OJ 287. We carried out *BVRI* observation of OJ 287 from 2003 September to 2008 May, using 0.6 m telescope of Sobaeksan Optical Astronomy Observatory, in Republic of Korea, and 1.0 m robotic telescope of Mt. Lemmon Optical Astronomy Observatory, in USA. During the monitoring campaign, the target shows strong flux variations of ΔB = 1.37 mag (14.20–15.57 mag), ΔV = 2.68 mag (13.71–16.39 mag), ΔR = 2.31 mag (13.30–15.61 mag), and ΔI = 2.19 mag (12.71–14.90 mag). We also investigate the variations of the colors. In order to analyse the variation correlations of the flux and the spectral index, we introduce a method to compare the variation rates of the two parameters. By comparing our results with the particle acceleration model of Kirk & Mastichiadis (1999), we suggest the possible emission mechanisms during the outburst.

Keywords. acceleration of particle — BL Lacertae objects : individual (OJ 287) — galaxies : active — radiation mechanisms : non-thermal — quasars : general

Table of Contents

List of Figures

List of Tables

Chapter 1

Introduction

Blazars belong to the extreme class of radio-loud active galactic nuclei (AGN). They show rapid and large variations throughout all electromagnetic spectrum, from the radio band up to γ–ray energies, with various variability timescales ranging from hours to years (Raiteri et al. 2008).

According to the unified model of AGN, the dominant non-thermal emission from the blazars are caused by the relativistic jets oriented close to the line of sight (see the reviews in Urry & Padovani (1995)). The low-energy non-thermal emission, from the radio band to X-ray frequencies, is due to synchrotron radiation, while the higher-energy emission, mostly γ -ray, is likely to be produced by inverse-Compton scattering (Raiteri et al. 2008).

Blazars include BL Lac objects (BL Lacs) and flat-spectrum radio quasars (FSRQs). Their observable characteristics are usually explained with the same physical mechanism of beamed emission from a relativistic jet aligned with our line of sight (Fiorucci et al. 2004). BL Lacs show featureless optical emission lines and non-thermal contribution due to synchrotron radiation. Meanwhile FSRQs show strong emission lines and a thermal contribution that is comparable to the synchrotron emission in the optical spectral region (Fiorucci et al. 2004).

BL Lacs can also be divided into the two sub-types characterized by different average properties (Padovani & Giommi 1995). High energy peaked BL Lacs (HBL) are the ones that emit most of their synchrotron power at high frequencies, from UV to X–ray, while low energy peaked BL Lacs (LBL) emit most of their synchrotron power at low frequencies, from optical to near-infrared bands. Several sources show intermediate behavior between the HBL and LBL classes, which are called Intermediate energy peaked BL Lacs (IBL).

OJ 287 (RA: $08^{\mathrm{h}}\,54^{\mathrm{m}}\,48.9^{\mathrm{s}}$, Dec: $+20^{\circ}\,06'\,31''$) is the typical LBL. Figure 1.1 shows the *V* band image of OJ 287 along with standard stars used in this study. It is one of the best studied BL Lacs which has been observed optically since the late nineteenth century (Valtonen et al. 2008b, see Figure 1.2).

The light curve reveals a highly active object which shows a large quasi-periodic optical outburst with an 12–year intervals, with two outburst peaks per interval (Sillanpää et al. 1988a; Lehto & Valtonen et al. 1996). The light curve of this period has been explained by a variety of models as follows : Lehto & Valtonen et al. (1996) proposed a model in which a secondary body (a black hole) pierces the accretion disk of the primary black hole and produces two impact flashes per period. Sillanpää et al. (1988a) suggested variations of the accretion rate in a disk, and Katz (1997) suggested variations of a wobble of a jet in a binary black hole system. Yet another models were suggested such as oscillations in an accretion disk (Igumenshchev & Abramowicz 1999) or oscillations in a jet (Hughes et al. 1998) of a single black hole.

International OJ–94 campaign confirmed 12-year period of OJ 287 (Sillanpää et al. 1996a,b). Pursimo et al. (2000) presented a result of intensive optical, infrared, and radio monitoring data taken between 1993 and 1998. These results show that the optical and infrared fluxes vary continuously with timescales ranging from tens of minutes to years. Valtonen et al. (2008a, 2008b) presented the 2005 outburst and the 2007 outburst in OJ 287 with precessing binary black hole model (Lehto & Valtonen et al. 1996; Sundelius et al. 1996, 1997; Valtonen 2007). Evidence for long-term variability behavior of optical spectral index with time was presented by Zheng et al. (2008), based on the published *U, B, V, R* and *I* band data. Fan et al. (2009) presented a optical photometry result of blazar OJ 287 from 2002 to 2007. Valtonen et al. (2009) analysed outbursts in OJ 287 during 2005–

2008 by considering the effect of varying emission from the jet caused by tidally induced variations in the accretion flow.

Multiwavelength observing campaigns from radio to X–ray frequencies are available for a limited number of objects, due to the difficulty of obtaining data with adequate time sampling and duration. The short snapshots of the targets result in the shortage of information about their mid- and long-term evolution. Recently, however, small-size and dedicated telescopes, in conjunction with international consortiums, have increased the amount of photometric data, sometimes with a fair continuous sampling during specific observing campaigns (Ciprini et al. 2007). We try to make use of multi-band variability studies limited to the optical range and one object with relatively long observing periods.

Although the optical bands have a narrow spectral extension, it can yield useful a clue to the emission nature, such as the synchrotron emission peak and other possible contributions, e.g., thermal emission from the accretion disk around the central engine, the emission from the surrounding regions of the nucleus, or the emission from the host galaxy. Moreover, historical light curve of blazar is available at optical wavelengths for several bright objects, although they are rather sporadic.

In this paper we present result of the blazar OJ 287 monitoring during six years from 2003 September to 2008 May. This quasi-simultaneous *BVRI* observations allowed us to study colors and the continuum spectrum as well as flux for mid- and long- term scales (days, weeks, years). The main aim of our paper is to investigate the flux variability behavior and spectral slope variability on the intermediate scales. In addition we try to discriminate among the various theoretical interpretations and understand the radiation mechanisms and physical features at emission region (Ciprini et al. 2007).

The data from 2003 to 2004 were already published in Gu et al. (2006). Some parts of data from 2005 to 2008 have been included in the Whole Earth Blazar Telescope (WEBT) campaign, but have not yet been published.

This paper is organized as follows: Observation and data reductions are described in chapter 2. In chapter 3, we present our results on flux variability, spectral variability and their correlation. In chapter 4, we discuss the results with respect to the existing theoretical models.

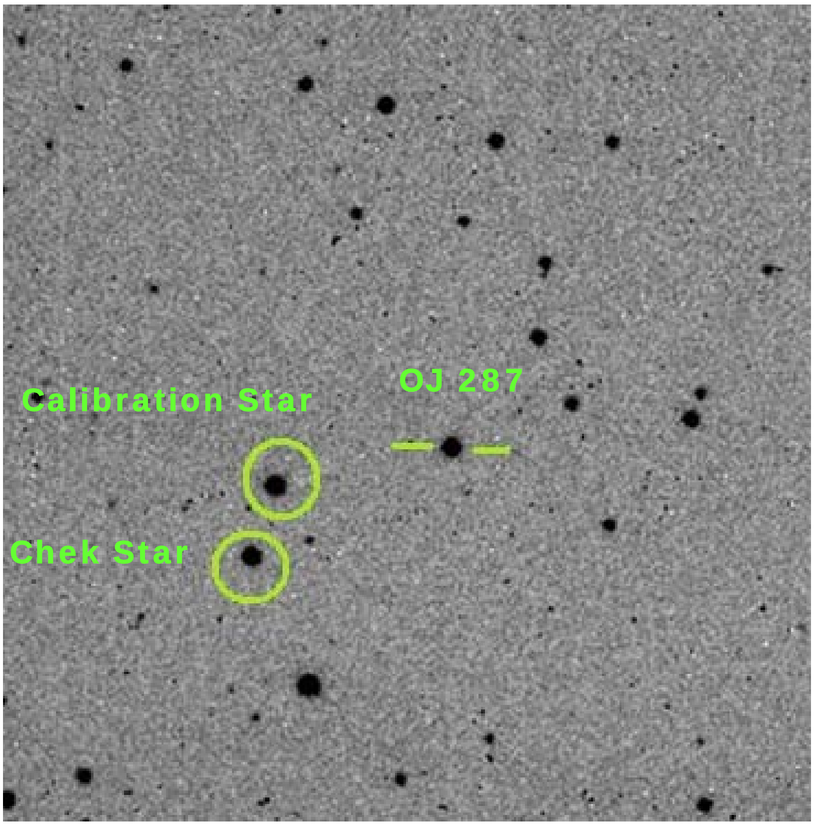

FIG. 1.1.—*V* band image for blazar OJ 287 from our study. The double bar represents the OJ 287 and the open circles represent the calibration star and check star used for calibration.

.

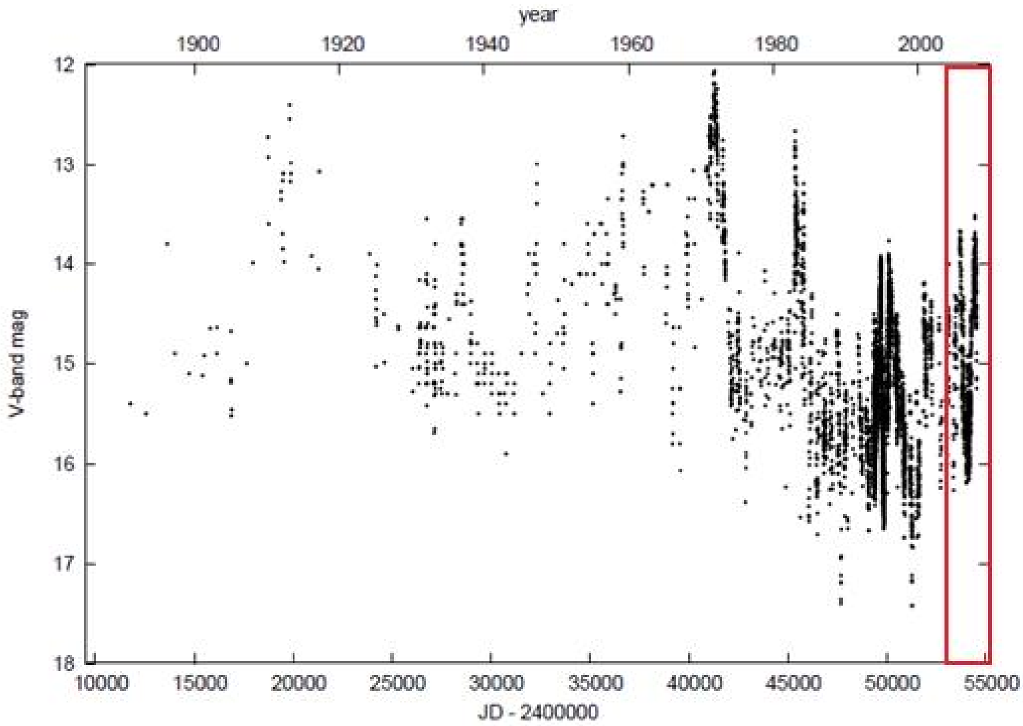

FIG. 1.2.—Historical light curve of OJ 287 in *V* band (Valtonen et al. 2008b). The red box shows the period when we performed our observation campaign.

.

Chapter 2

Observation and data reduction

We carried out *BVRI* optical monitoring of blazar OJ 287 using the 0.6 m telescope at Sobaeksan Optical Astronomy Observatory (SOAO) in the Republic of Korea for 27 nights, and *BVRI* observation with the 1.0 m robotic telescope at Mt. Lemmon Optical Astronomy Observatory (LOAO) in Arizona, USA, for 36 nights. The observation logs are summarized in Table 2.1. To check the long-term and short-term variability, we tried to make observation at least seven nights a month. Continuous optical monitoring was possible by using two telescopes at different longitudes. Each telescope was equipped with CCD cameras, and *BV* (Johnson) and *RI* (Cousins) filter sets. The significance of our data is that observations were carried out with same CCD cameras and filter sets at SOAO and LOAO in 2003–2008.

Typical integration times were 300, 250, 150 and 120 seconds for the *B, V, R* and *I* filters, respectively. However, different exposure times were applied according to the seeing and weather conditions for each night. During observation, we tried to put each target object at the same location on the CCD surface within a few pixels, in order to achieve efficient photometry. Twilight flat images were taken at both dusk and dawn when available, and the bias and dark images were taken at the beginning and end of the observations.

We selected two standard stars : No. 12 and No. 13 in González-Pérez et al. (2001). Aperture photometry was carried out for OJ 287 and all standard stars with APPHOT package in IRAF[1]. The measuring apertures were set to include the total flux of the stars. The seeing condition varies for each observation run, and there is a trend of the instrumental magnitude variations with the FWHM variations of a star from night to night (Clements & Carini 2001). In order to correct the seeing variation effect, and to try to include the total flux from object when seeing varies, we set the radius of the measuring aperture to be proportional to the FWHM of non-staturated images of bright isolated stars in the frames during one night (Lee et al. 2003). After experimenting with various aperture sizes, we set the aperture radius to be $4 \times$ FWHM, the inner radius of the sky annulus to be at 10 pixel, and the width of the sky annulus to be 15 pixels, to maximize the S/N ratio (Gu

[1] IRAF is distributed by the National Optical Astronomy observatory, which is operated by the Association of Universities for Research in Astronomy, Inc., under cooperative agreement with the National Science Foundation.

et al. 2006). The FWHMs at two observatories varied from 2.″5 to 3.″0 in average. The sky annulus is not large enough from the images considering the FWHMs. Therefore it is possible that the measurements yielded fainter magnitudes. However the bias is not significant in the differential photometry in this study.

The observation errors are estimated from the rms differential magnitude between the calibration star and another standard star used for checking :

$$\sigma = \sqrt{\frac{\sum(m_i - \overline{m})^2}{N - 1}}$$

where is $m_i = (m_c - m_K)_i$ is the magnitude difference between the calibration star *C*, No. 13, and check star *K*, No. 12, while $\overline{m} = \overline{m_C - m_K}$ is the average of magnitude difference for the entire data set, and *N* is the number of observations on a given night (Gu et al. 2006). For each measurement, the typical rms error is between 0.01 and 0.03 mag.

A total of 2738 *BVRI* photometric points were obtained during 59 nights (see Table 2.2). Data sets from two observatories are roughly in agreement with each data within the uncertainties. Figure 2.1 shows that our results are in good agreement with the data taken at same epochs from American Association of Variable Star Observers (AAVSO) International Database[2].

---

[2] http://www.aavso.org

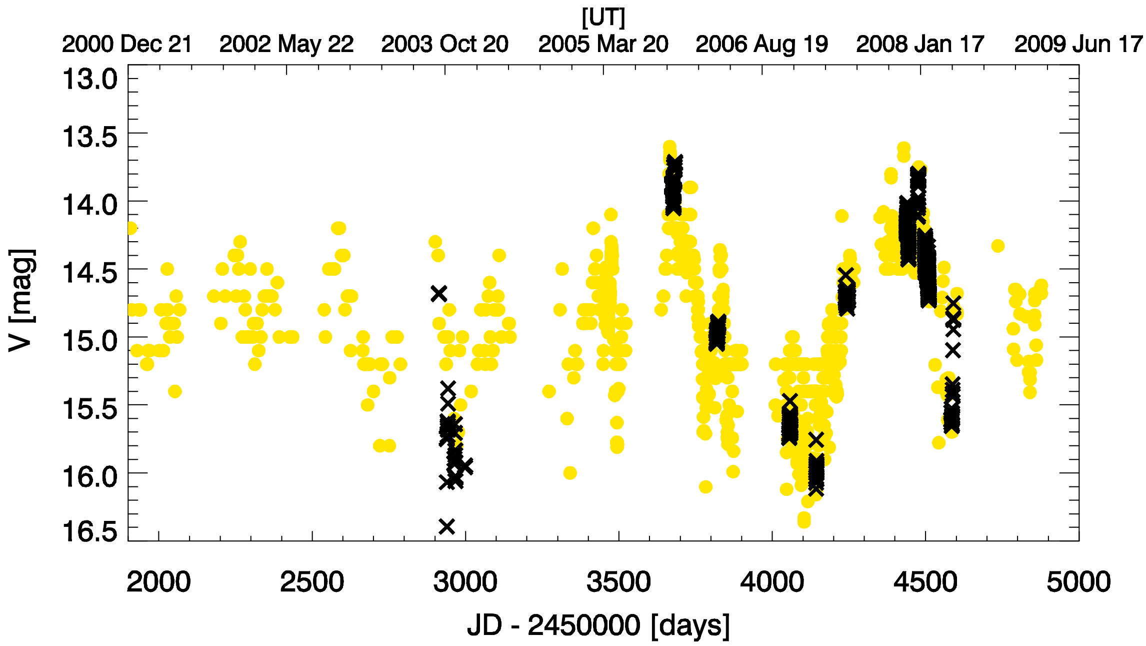

FIG. 2.1.—*V* band light curve of OJ 287 in 2001–2009. The closed circles represent the data from American Association of Variable Star Observers (AAVSO) International Database and the crosses represent the data from our observations.

TABLE 2.1.—Log of observation from 2003 September to 2008 May.

Date (Julian Date – 2450000)	Date	Filter	
		LOAO	SOAO
2913	2003 Sep	*VRI*	
2939-2943	2003 Oct	*VRI*	*VRI*
2953-2967	2003 Nov	*VRI*	*VRI*
2998	2003 Dec		*VRI*
3673-3674	2005 Oct	*BVRI*	
3676-3682	2005 Nov	*BVRI*	
3818-3824	2006 Mar	*BVRI*	
4055-4058	2006 Nov		*VRI*
4143-4144	2007 Feb		*VRI*
4181-4182	2007 Mar		*R*
4239-4246	2007 May	*BVRI*	
4437-4444	2007 Dec	*BVRI*	*VRI*
4474-4476	2008 Jan	*BVRI*	*VRI*
4497-4510	2008 Jan–Feb	*BVRI*	*VRI*
4583-4587	2008 Apr		*VRI*
4588-4590	2008 May		*VRI*

TABLE 2.2.—Number of photometric *BVRI* data points of blazar OJ 287 obtained by each observatory from 2003 September to 2008 May.

Observatory	***B***	***V***	***R***	***I***	**Total**
LOAO	473	478	487	491	1929
SOAO	0	256	301	252	809
Total	473	734	788	743	2738

Chapter 3

Results

3.1 Flux variability

During our observing runs, the overall magnitude variations were ΔB = 1.37 mag (14.20–15.57 mag), ΔV = 2.68 mag (13.71–16.39 mag), ΔR = 2.31 mag (13.30–15.61 mag), and ΔI = 2.19 mag (12.71–14.90 mag). In the V band, our data have the brightest state of 13.71 mag on JD 2453682 in 2005 November and the faintest state of 16.39 mag in JD 2452939 in 2003 October. A similar result was reported by Valtonen et al. (2008a) who showed a maximum at V = 13.6 mag between JD 2453679 and JD 2453683 based on their data from 2005 January to 2006 June.

Our observed optical light curves in the *BVRI* bands of blazer OJ 287 (Figure 3.1) show a clear double-peak structure with the first peak occurred in 2005 November and the second peak in 2008 January. By comparing results reported by Valtonen et al. (2008a), we can confirm the quite similar timing of the first peak. Our second peak, however, does not correspond to the maximum peak which was measured by Valtonen et al. (2008b, 2009). Pusimo et al. (2000) reported that the second peak of OJ 287 in 1996 is broader than the first peak. Our observations could not cover the whole expected period of the second outburst.

During the outburst periods, our data show flaring activities in time scales from hours to week which were also identified in the previous outbursts in 1994–1997 (Pursimo et al. 2000). It is also evident that this flaring activity continues after the outbursts, but with smaller variabilities in frequency and amplitude.

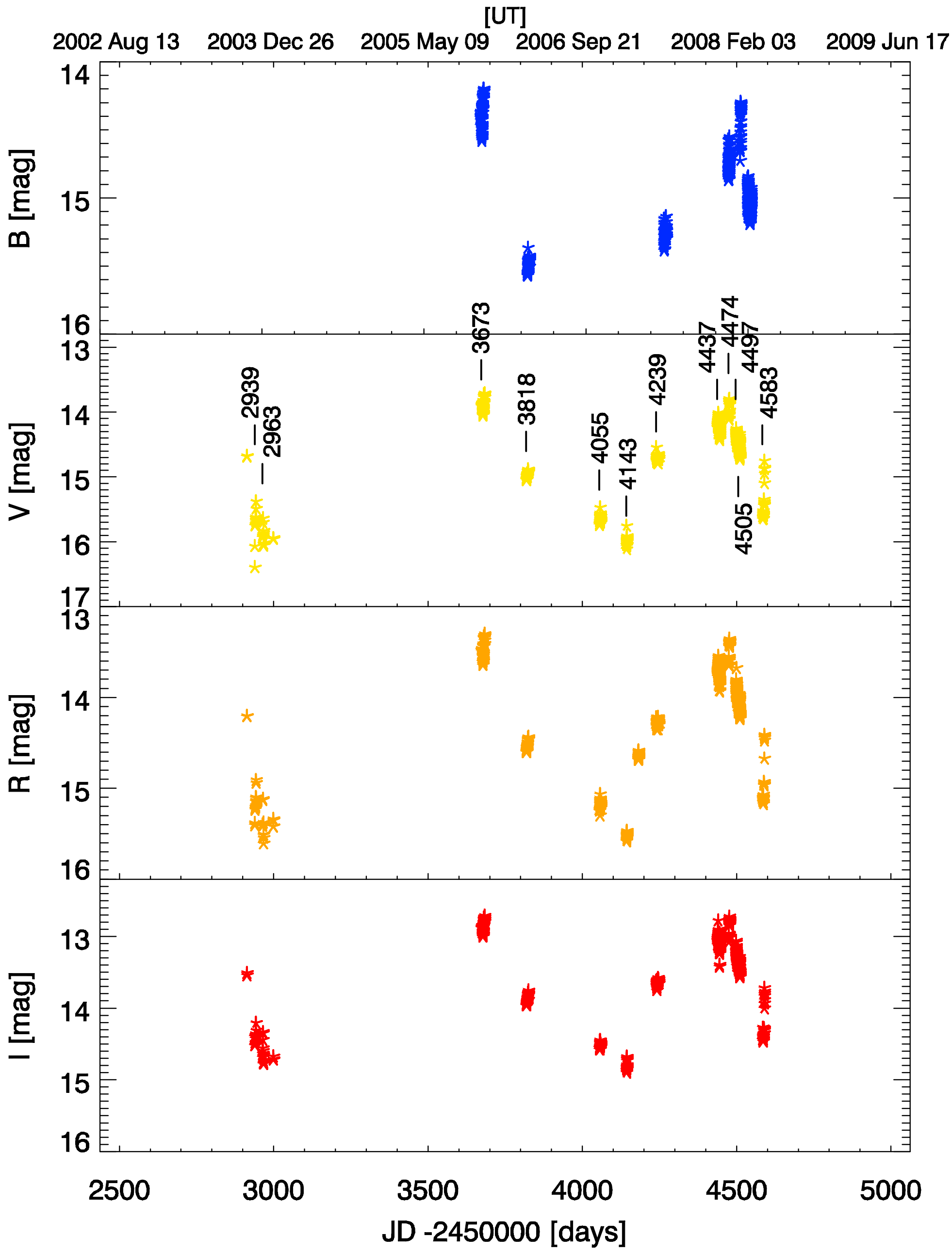

FIG. 3.1.—Light curves of blazar OJ 287 in the *BVRI* bands from 2003 September to 2008 May. We grouped the data based on the continuity of nights, and marked with the Julian Date (–2450000) of the beginning night in the group.

3.2 Spectral variability

The continuum spectral flux distribution of blazars in the optical bands can discriminate the emission components such as synchrotron and thermal radiation. In addition the correlation between the optical flux variations and the spectral index variations can reveal the detailed emission mechanisms (Ciprini et al. 2007).

In calculation the color indices, we grouped the passband filter measurements whose time gabs in the sequence are shorter than 15 minutes, in order to reduce possible intrinsic micro-variations. It is generally the case that the spectral energy distribution can be described by a typical synchrotron power law, $F_{\nu} = \nu^{-\alpha}$. We derive the spectral index, $\alpha_{VR,}$ from the color index, $(m_V – m_R)$,

$$\alpha_{VR} = -\frac{\log\left(f_{\nu_V}/f_{\nu_R}\right)}{\log(\nu_V/\nu_R)} = 2 + \frac{\log\left(f_{\lambda_V}/f_{\lambda_R}\right) - \frac{(m_V - m_R)}{2.5}}{\log(\lambda_R/\lambda_V)},$$

where the effective wavelengths, λ_V and λ_R are 0.55 μm and 0.71 μm, respectively (Cox 2000).

Figure 3.2 shows the light curves of the R band flux and the spectral index. The spectral index values in 2003–2008 varies from –0.4 to 1.5. We can notice the significant variabilities of the spectral index during the flares. On the other hand, the long-term spectral variability in our data seems achromatic. Recently, by analysing between the long-term spectral index and the flux in 1972 –2006 , Zheng et al. (2008) showed that the spectral index variability period is agree with the optical flux variability period of about 11.96 year and the time lag between the optical spectral index and the optical flux density is half of the flux variability period, 5.48 year.

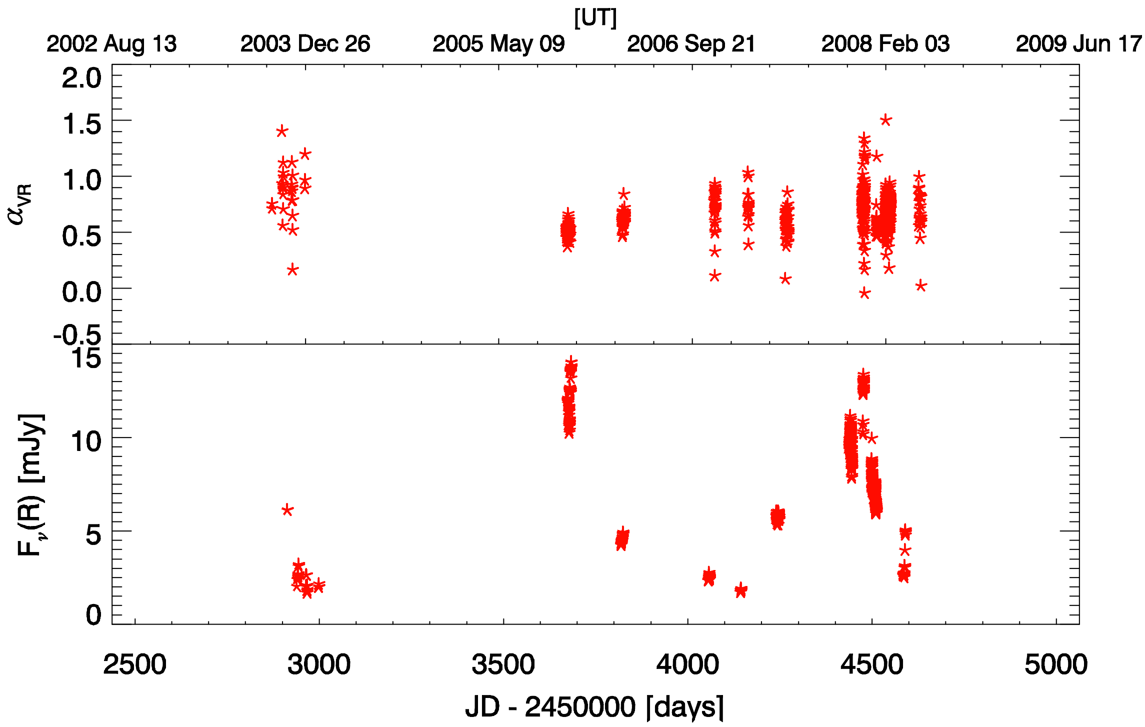

FIG. 3.2.—Light curves of the spectral index α_{VR} and the *R* band flux in blazar OJ 287.

3.3 Correlation between α_{VR} and $F_\nu(R)$

The correlation between the spectral index and the flux of the blazar OJ 287 in optical band can be compared with other similar studies (Takalo & Sillanpää 1989; D'Amicis et al. 2002; Vagnetti et al. 2003; Fiorucci et al. 2004; Gu et al. 2006; Zheng et al. 2008). In these studies, the spectrum becomes bluer (flatter) when the source is brighter. On the other hand, Zheng et al. (2007) presented an opposite case when the brightness increases, the optical spectra becomes redder.

From our photometric data, we have analysed the correlation between the spectral index and the R band flux density (see Figure 3.3), we calculate the relationship between α and $F_\nu(R)$, with linear regression, as

$$\alpha = 0.764 - 0.013\ F_\nu(R).$$

The correlation coefficient indicates r = –0.26 with a probability less than 1×10^{-2} that no correlation is present. This correlation implies that the spectrum becomes bluer (flatter) when the source is brighter. And this result is in accord with the common color change tendency in blazars.

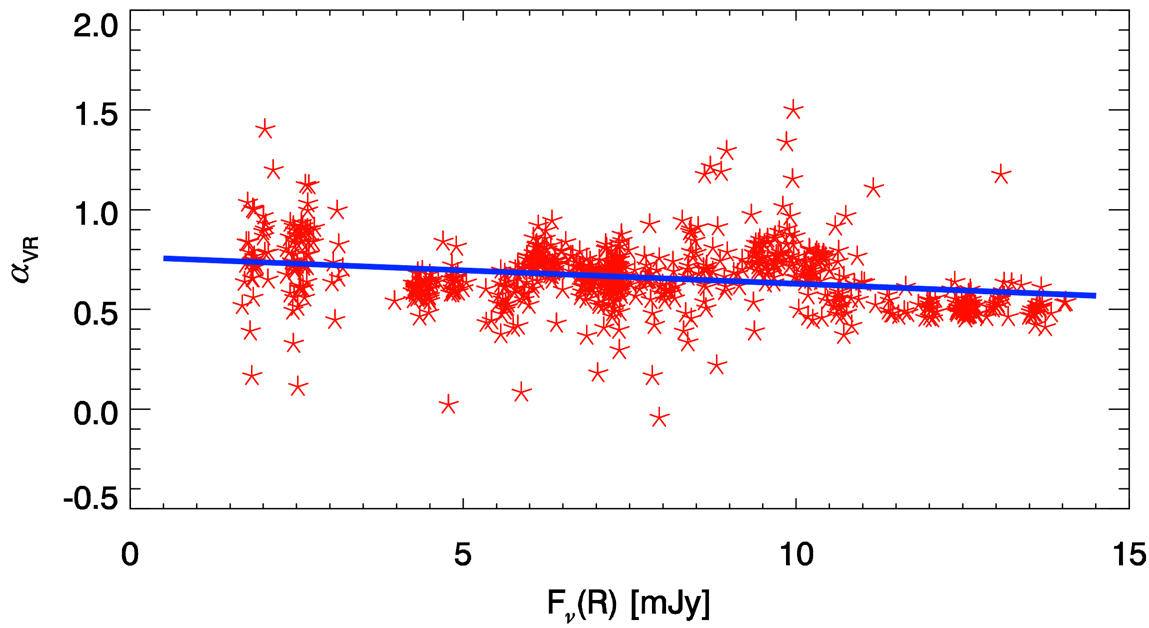

FIG. 3.3.—Instantaneous spectral index α_{VR} verse specific flux at the effective frequency of the observed *R* band for blazar OJ 287. This shows a general trend in blazars that the spectrum becomes bluer (flatter) when the source is brighter. The regression line is also shown in blue color.

Chapter 4

Discussion

4.1. Pattern of the spectral index and the flux density

In most cases, the blazar OJ 287 tends to be bluer when brighter. However, spectral slope changes differ quantitatively patterns according to observation dates of object (Ciprini et al. 2007). In recent years, many other investigators have studied about these patterns. During well-defined and large flares at X–ray bands, especially observed in HBL, the X-ray spectral index versus the flux frequently displays a characteristic loop-like pattern (Georganopoulos & Marscher 1998; Kataoka et al. 2000; Ravasio et al. 2004). That pattern outlines a hysteresis cycle arising whenever the spectral slope is completely controlled by radiative cooling processes, mostly synchrotron and inverse-Compton (Kirk et al. 1998; Kirk & Mastichiadis 1999; Böttcher & Chiang 2002). In a few sources, e.g. PKS 0735+178, 3C 66A, GC 0108+224 and S5 0716+174, this feature was found in the optical bands too (Fiorucci et al. 2004; Ciprini et al. 2004, 2007). (Ciprini et al. 2007).

Ciprini et al. (2007) claims that around and beyond the synchrotron peak frequency, the behavior of the LBL sources during flares in the optical band is scaled in frequency, but possibly very similar to the course of the HBL in X-ray bands. Consequently variation at higher frequency band could lead those at the lower frequency bands during both the increasing and decreasing brightness phases, reflecting differences in electron cooling times.

In Table 4.1, Column 1 is the average Julian date per day, Column 2 is the average flux density per day, $<F_{\nu}(R)>$, Column 3 is the root-mean-square of flux density during the day, $RMS_{F,}$ Column 4 is the average spectral index per day, $<\alpha_{VR}>$, and Column 5 is the root-mean-square of spectral index during the day, σ_{α}. We grouped the data based on the continuity of nights, and marked with the Julian Date (–2450000) of the beginning night in the group and plot the average spectral index per day, $\overline{\alpha_{VR}}$, versus average *R* band flux density per day, $\overline{F_{\nu}(R)}$, from an continuous arbitrary 12 observing runs.

In our result, from Figure 4.1 to Figure 4.12, the evolution of spectral index as a function of the flux is unpredictable and did not show evident hysteresis loops by non-thermal cooling (Ciprini et al. 2007). The rather limited amplitude of the optical variability in the epochs, the possible superimposition of different emission processes in the optical band, the under-sampling, and the error propagation in the α calculation can be the main reasons for the lack of well-defined loops in such spectral index vs. flux diagrams (Ciprini et al. 2007). Our data are not sufficient to make a final judgment, and an improved multi-band monitoring and a better data sampling would probably clarify the existence of those patterns during variability in this object (Ciprini et al. 2007).

4.2. Variation rates of the spectral index and the flux density

Kirk & Mastichiadis (1999), one of the theoretical models, suggested that the acceleration of electrons at a shock front can produce loop-like characteristic patterns in the variation of the spectral index of the synchrotron emission as a function of flux. To analyse the possible variability patterns, Kirk & Mastichiadis (1999) choose the time-dependence of the rate at which electrons are picked up by the shock so as to mimic a flare of duration t_{var}. Thus, three time scales arise in the problem and suppose to the variability time t_{var}, the (energy independent) acceleration time t_{acc} and the synchrotron cooling time t_{cool}, which is inversely proportional to the particle energy. Three cases were divided into time and showed the Figure 4.26. In case I, $t_{cool} \gg t_{var} \gg t_{acc}$, acceleration can be regarded as essentially instantaneous, so that just the relatively slow cooling of varying injection spectrum is observed. This case result from soft lag because the cooling time decreases with energy. And the time scale of variation is roughly the same for both the rise and fall. This behavior is seen in both the synchrotron and the inverse-Compton components. In case II , $t_{cool} \gg t_{acc} \gg t_{var}$, the intensity shows a much faster rise than fall, together with a soft lag. It can be an indicator of a first-order Fermi acceleration mechanism at a shock front. These situation $t_{cool} \gg t_{acc}$ can occur only for electrons emitting well below the maximum frequency. However, the case III, $t_{cool} \approx t_{acc} \approx t_{var}$, can occur in close to the maximum frequency and shows hard lag which means a change in the number of particles picked up makes itself felt as a change in the number arriving at the relevant energy from lower energies, rather than the number cooling to the relevant energy from higher energies. Also it appears more clearly in the synchrotron flux than in the inverse-Compton component, because the highest energy electrons suffer most from the Klein-Neshina reduction in the scattering cross section. In conclusion, the important features which help to classify these patterns are the symmetry/asymmetry of the time profile and the character (hard or soft lag) of the spectral index behavior (Kirk & Mastichiadis 1999).

In order to quantify correlation between the spectral change and the flux variation, we investigate correlation coefficient plotted spectral index change versus flux density variation as a function of time (see Figure 4.13–Figure 4.25). The results are listed in Table 4.2. Column 1 is Julian date, Column 2 is the number of data points used for calculation the spectral index between *V* and *R* bands, Column 3 is the slope of linear regression, Column 4 is the linear correlation coefficient and Column 5 is the probability that no correlation is present. In our results, it can be seen that there are no uniform trends of variability ratios between spectral index α_{VR} and flux intensity $F_{\nu}(R)$. Interestingly, we find significant positive correlation of variability ratios for JD 2452963–2452966, JD 2453673–2453682, JD 2453818–2453823, JD 2454437–2454444, JD 2454497–2454500, and JD 2454505–2454510. The JD 2454055–2454058 and JD 2454239–2454246 are relatively weak, but still significant. However, no significant correlation is found for JD 2452939–2452943, JD 2454143–2454144, JD 2454474–2454476 and JD 2454583–2454590.

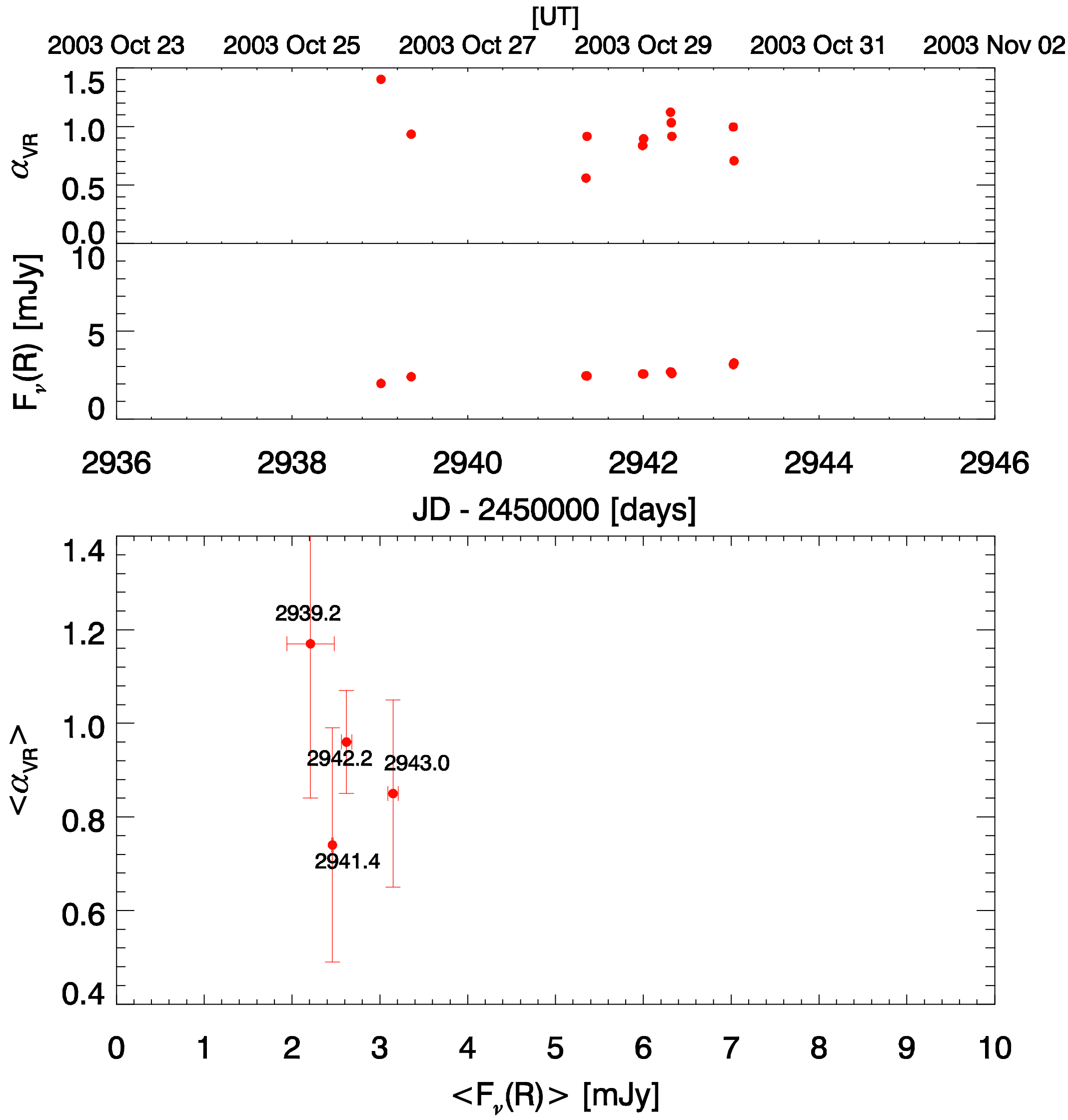

FIG. 4.1.—*Upper panel*: light curves of the spectral index α_{VR} and the flux $F_\nu(R)$ in blazar OJ 287. *Lower Panel:* evolution of the average spectral index per day, $<\alpha_{VR}>$, as a function of the average *R* band flux density per day, $<F_\nu(R)>$. The error bars show the root-mean-square of the data during the day (see Table 3.1.). The data were observed from JD 2452939 to JD 2452943.

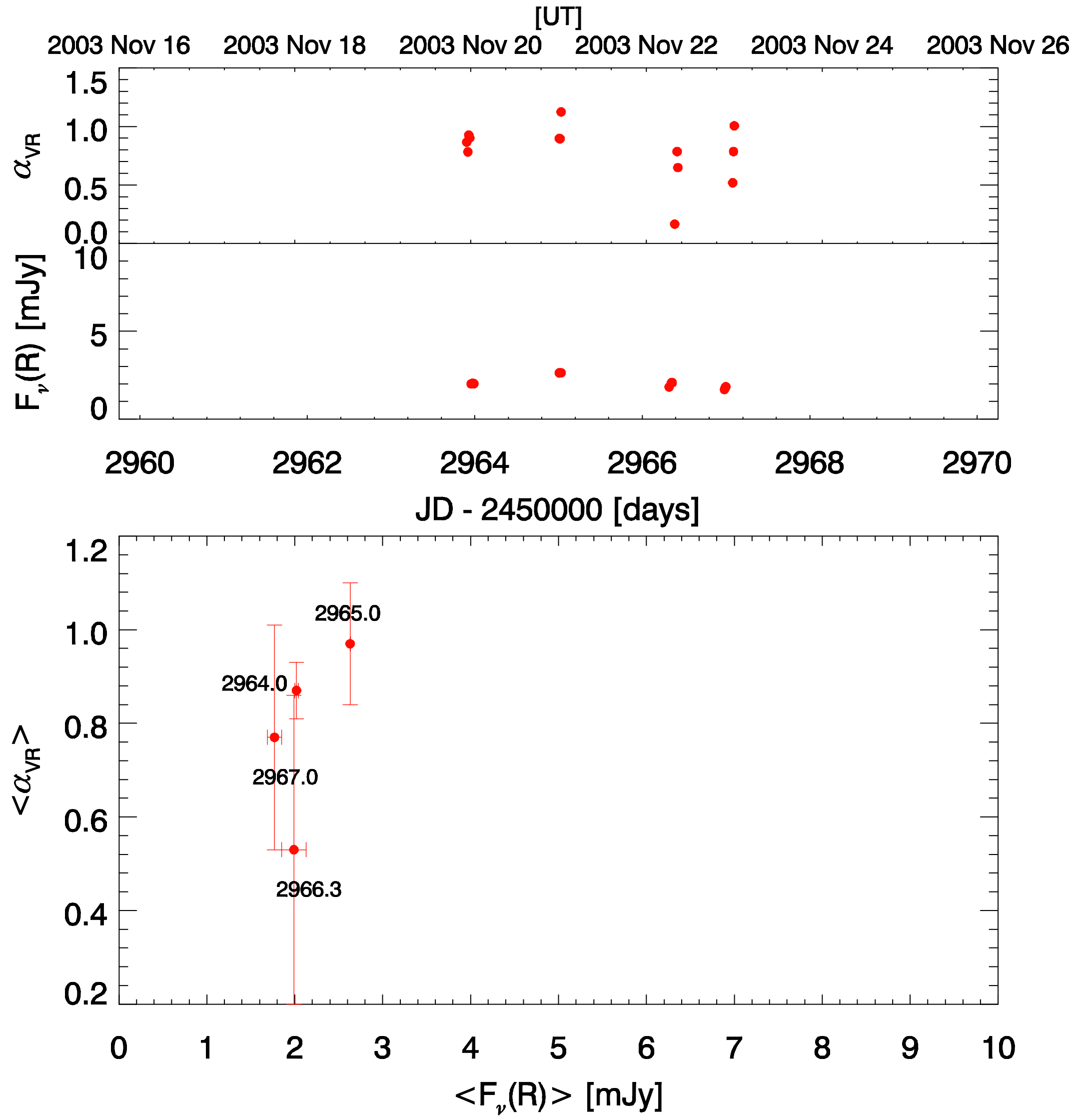

FIG. 4.2.—Same as in Figure. 3.4. The data were observed from JD 2452963 to JD 2452966.

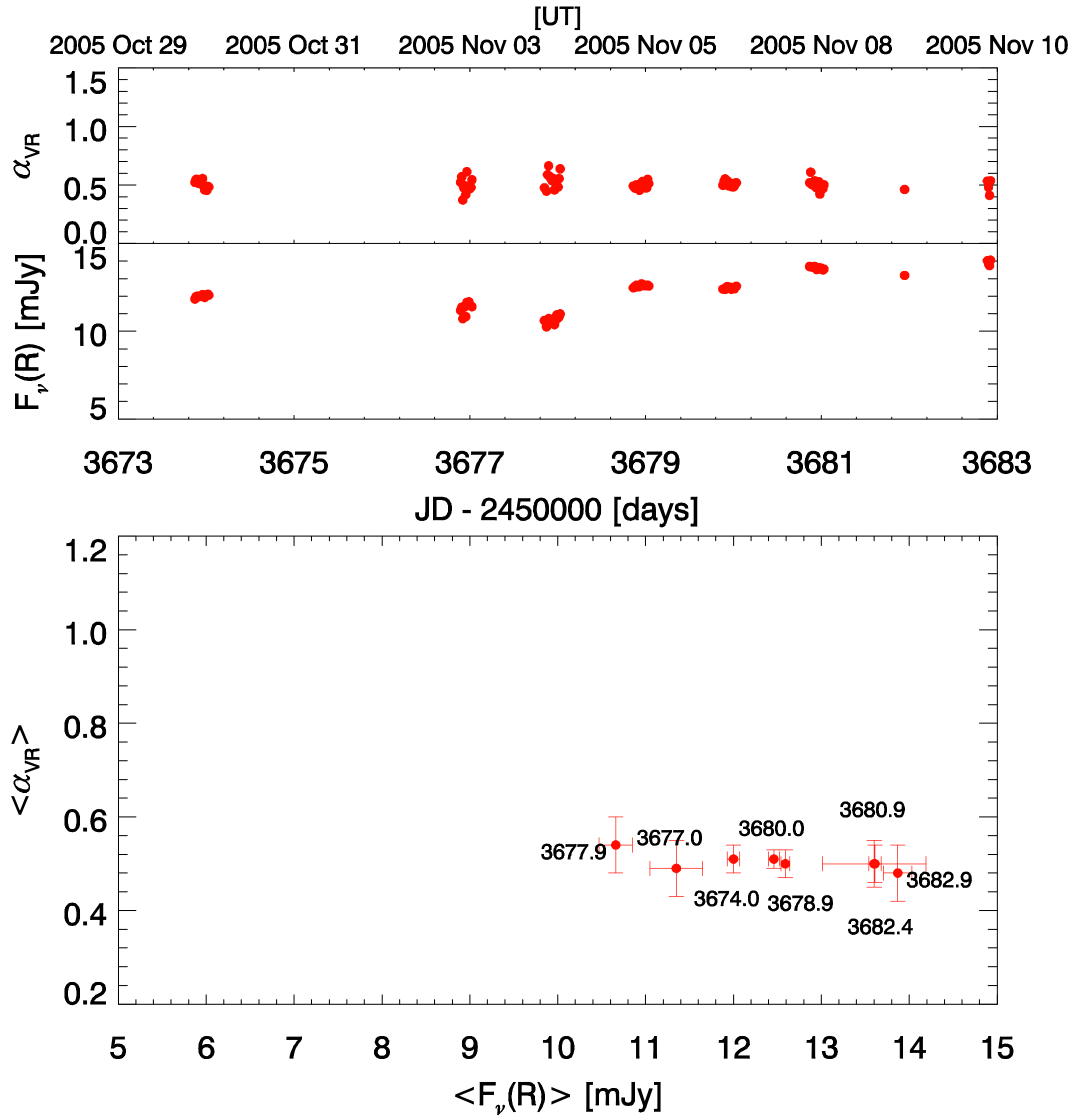

FIG. 4.3.—Same as in Figure 3.4. The data were observed from JD 2453673 to JD 2453682.

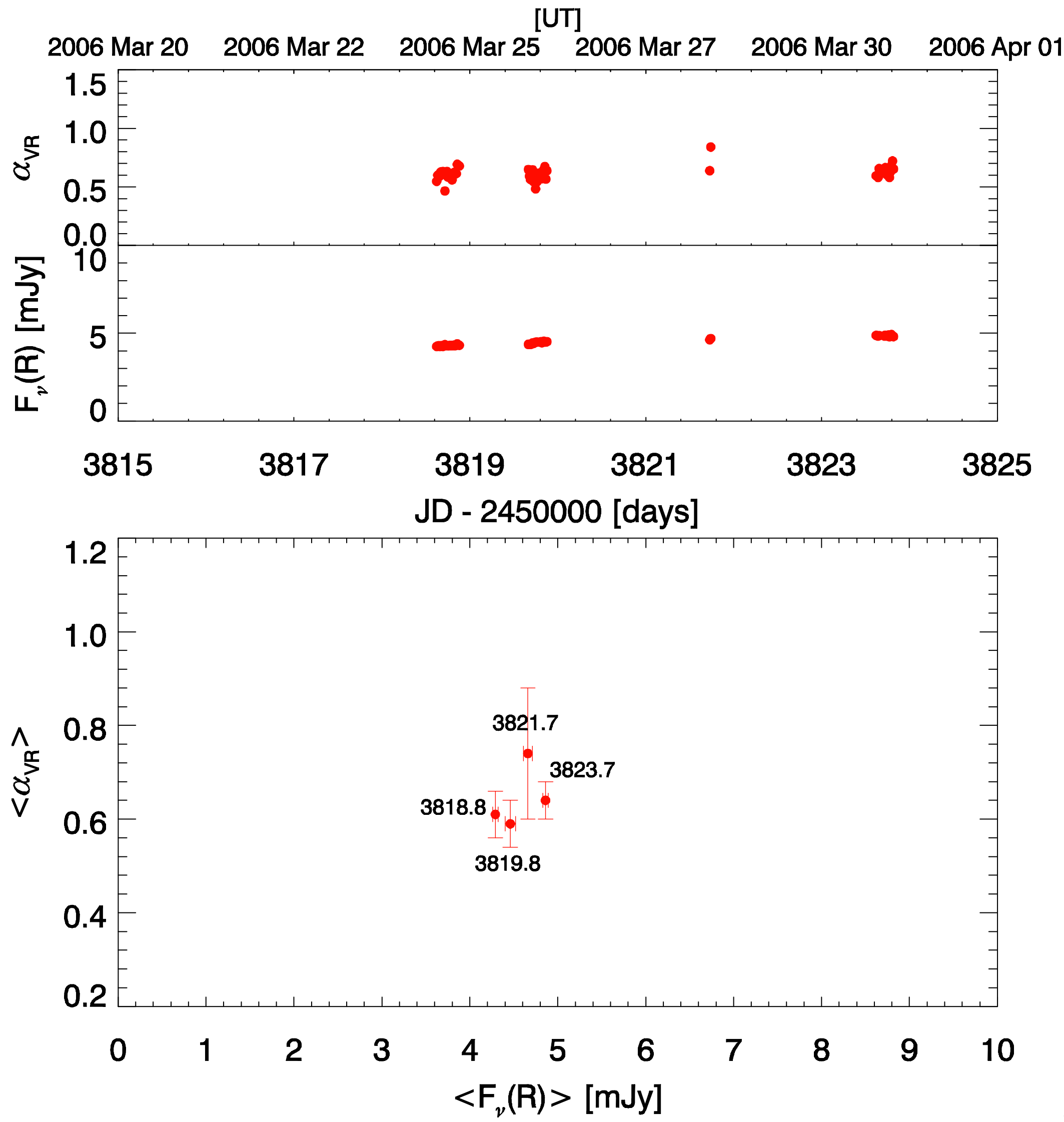

FIG. 4.4.—Same as in Figure 3.4. The data were observed from JD 2453818 to JD 24523823.

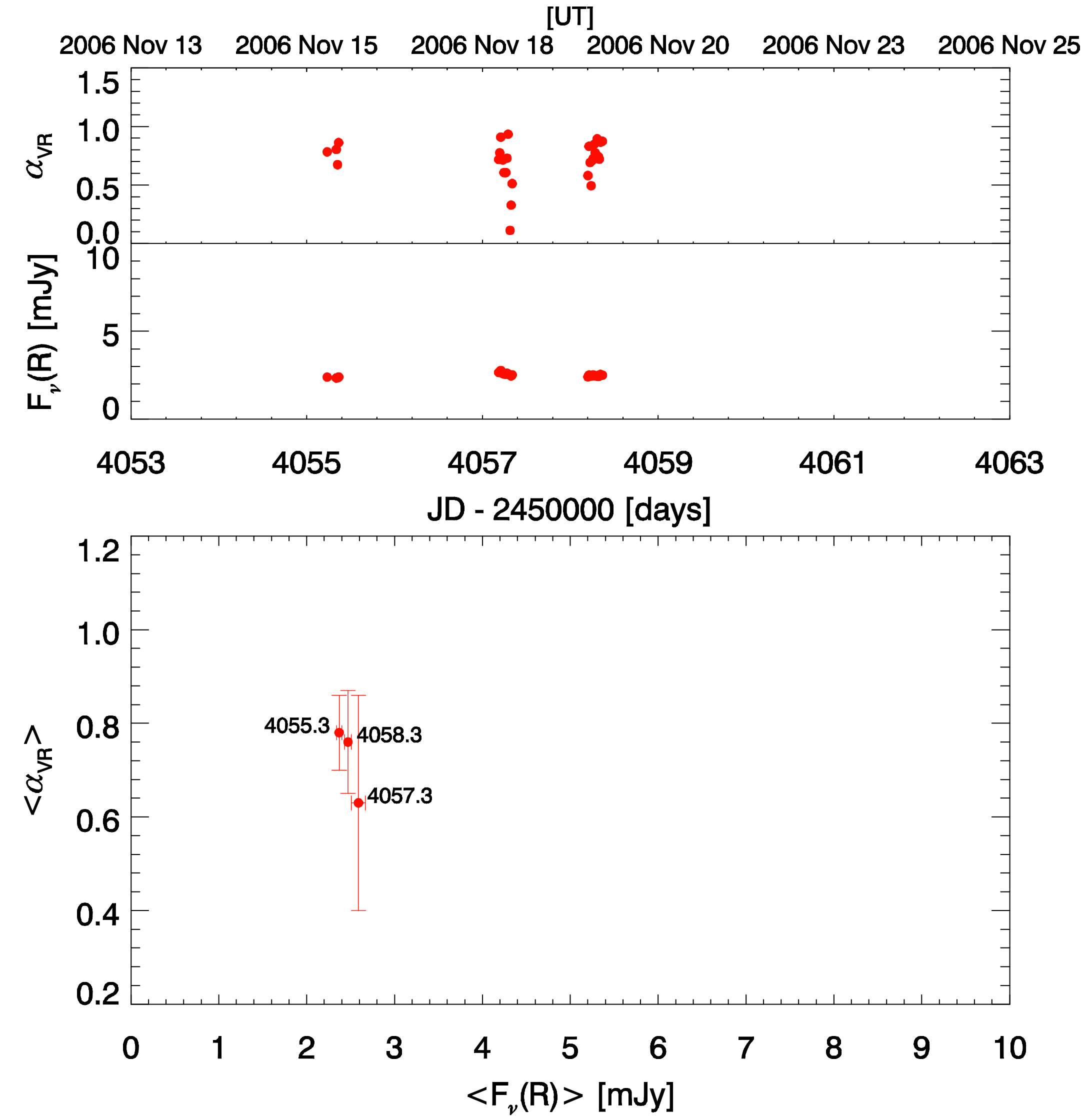

FIG. 4.5.—Same as in Figure 3.4. The data were observed from JD 2454055 to JD 24524058.

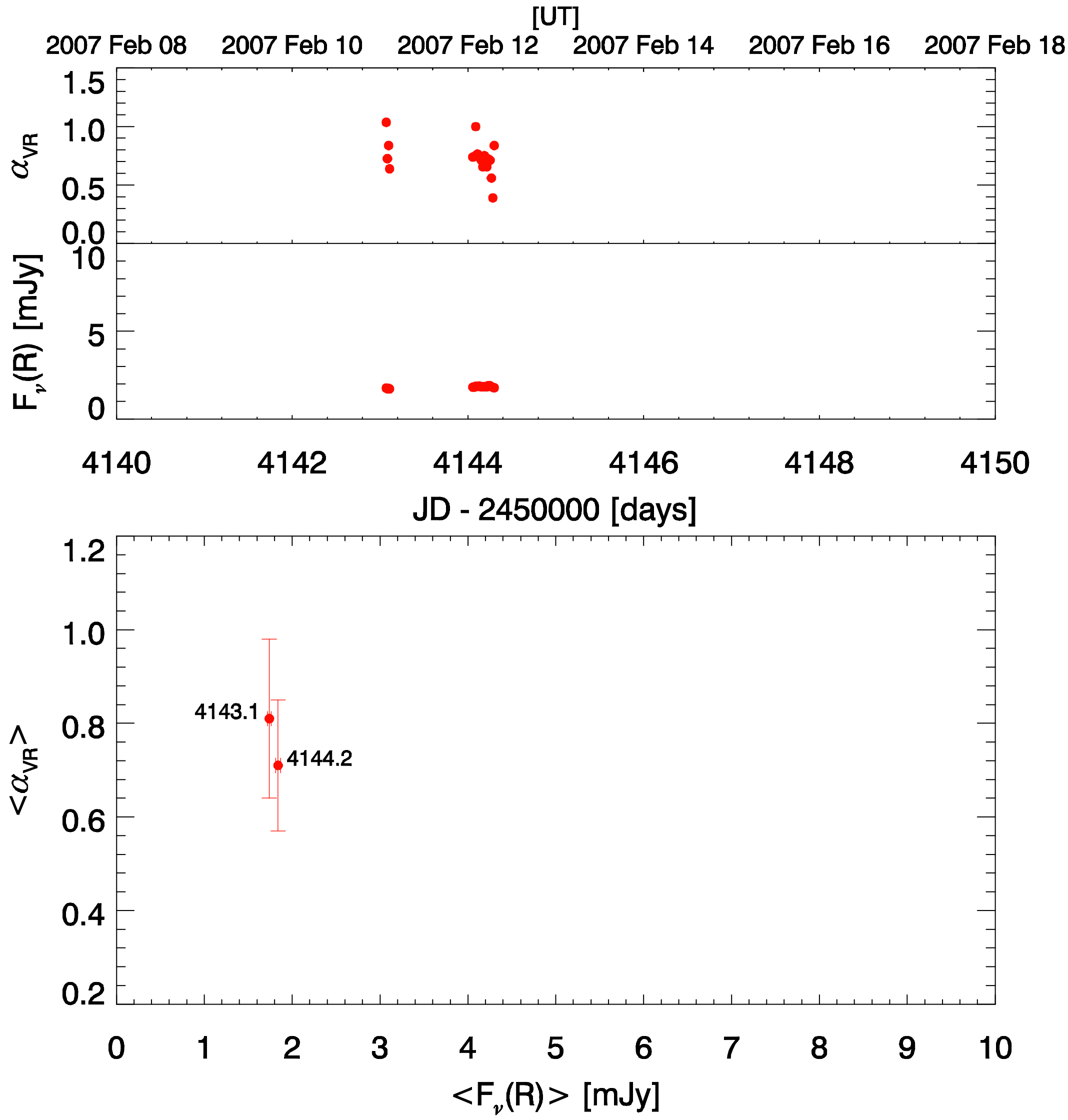

FIG. 4.6.—Same as in Figure 3.4. The data were observed from JD 2454143 to JD 24524144.

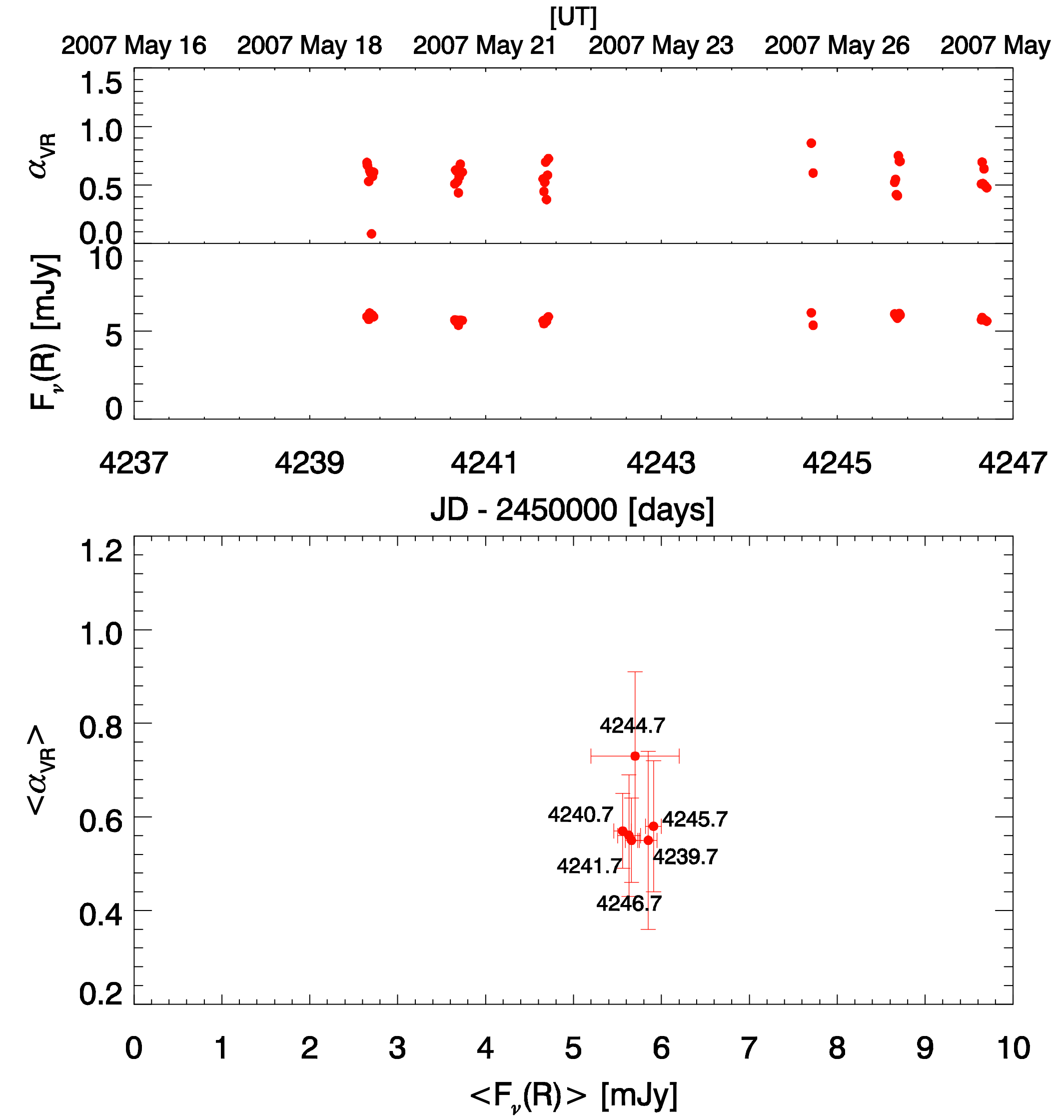

FIG. 4.7.—Same as in Figure 3.4. The data were observed from JD 2454239 to JD 24524246.

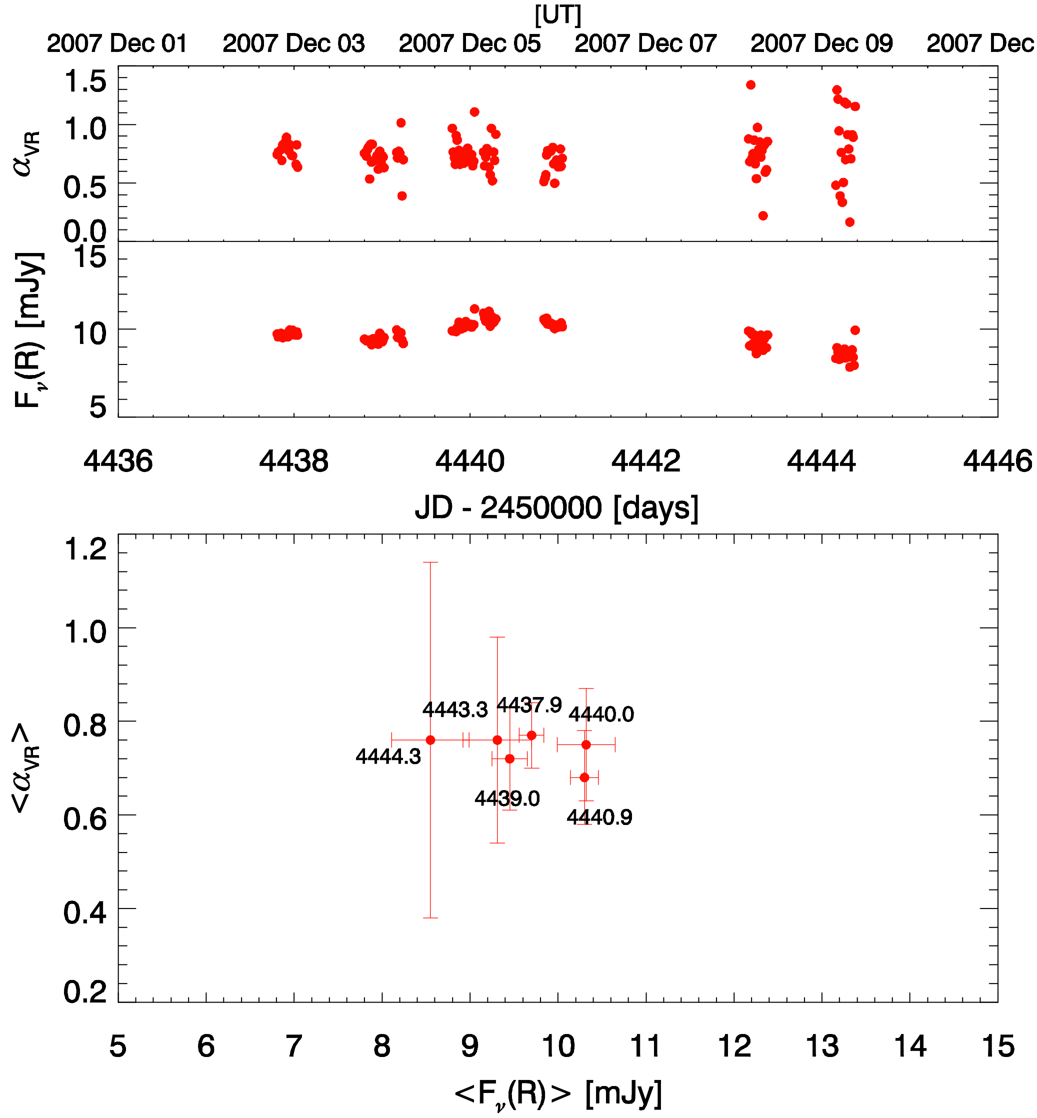

FIG. 4.8.—Same as in Figure 3.4. The data were observed from JD 2454437 to JD 24524444.

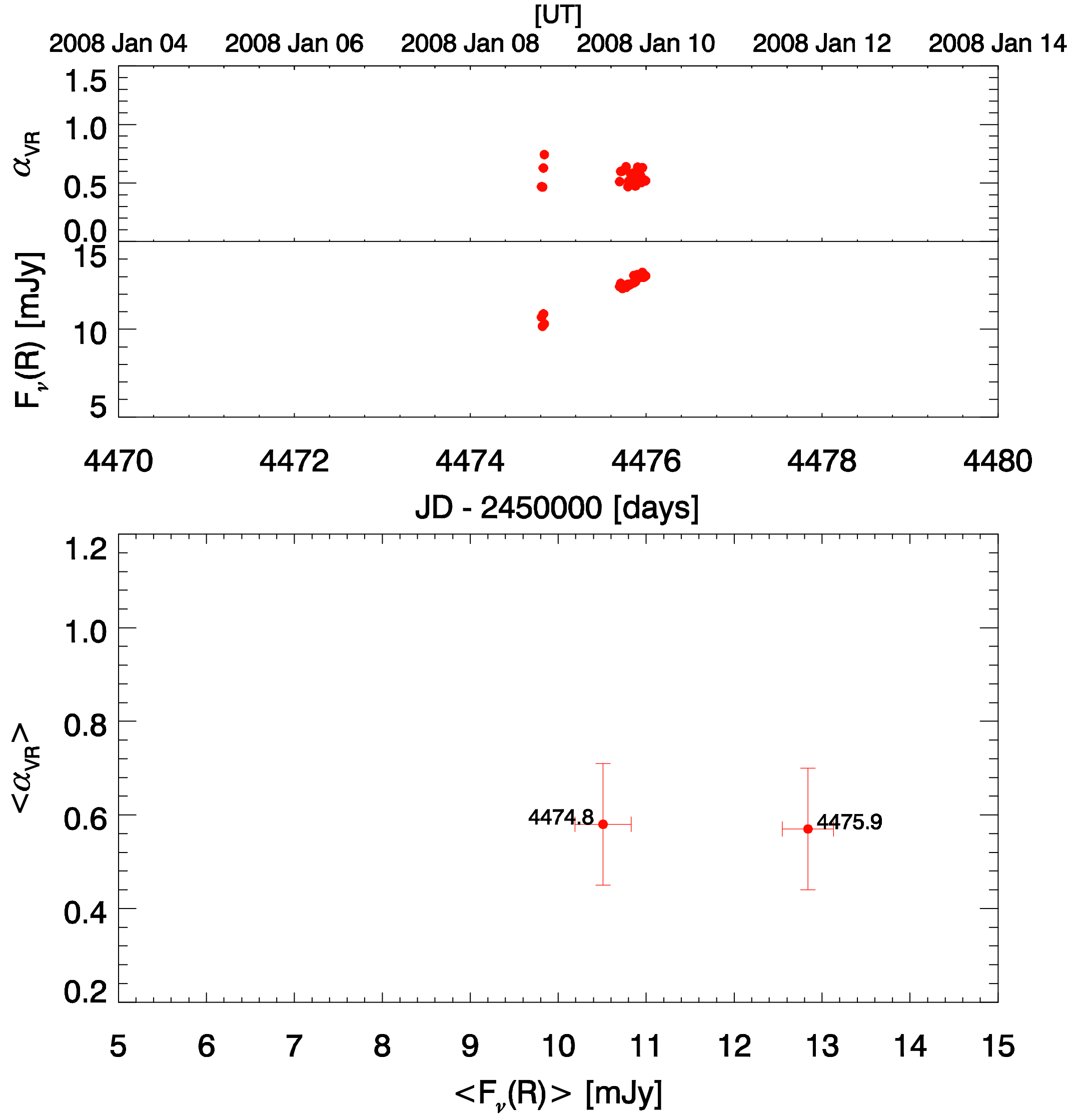

FIG. 4.9.—Same as in Figure 3.4. The data were observed from JD 2454474 to JD 24524476.

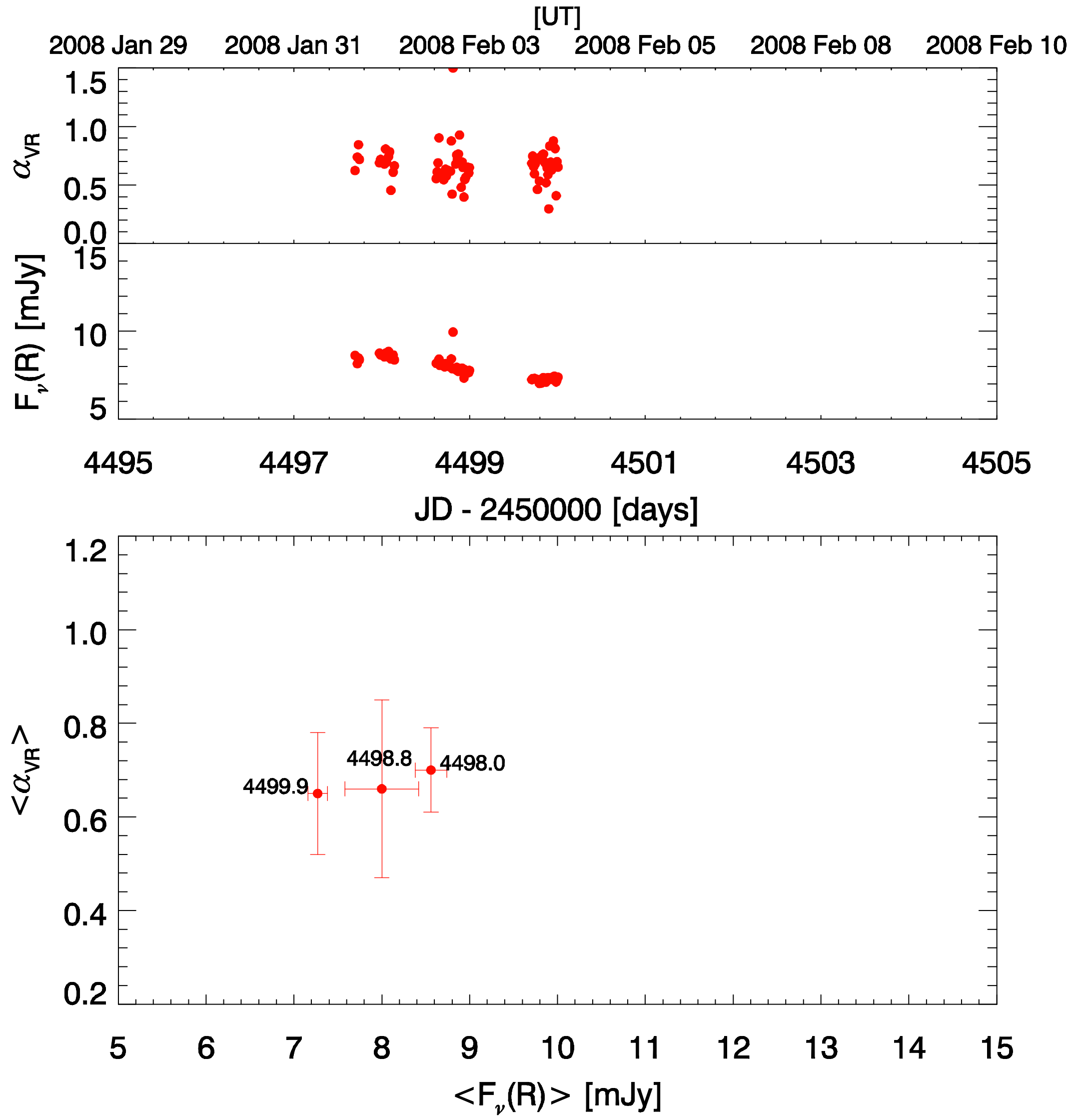

FIG. 4.10.—Same as in Figure 3.4. The data were observed from JD 2454497 to JD 24524500.

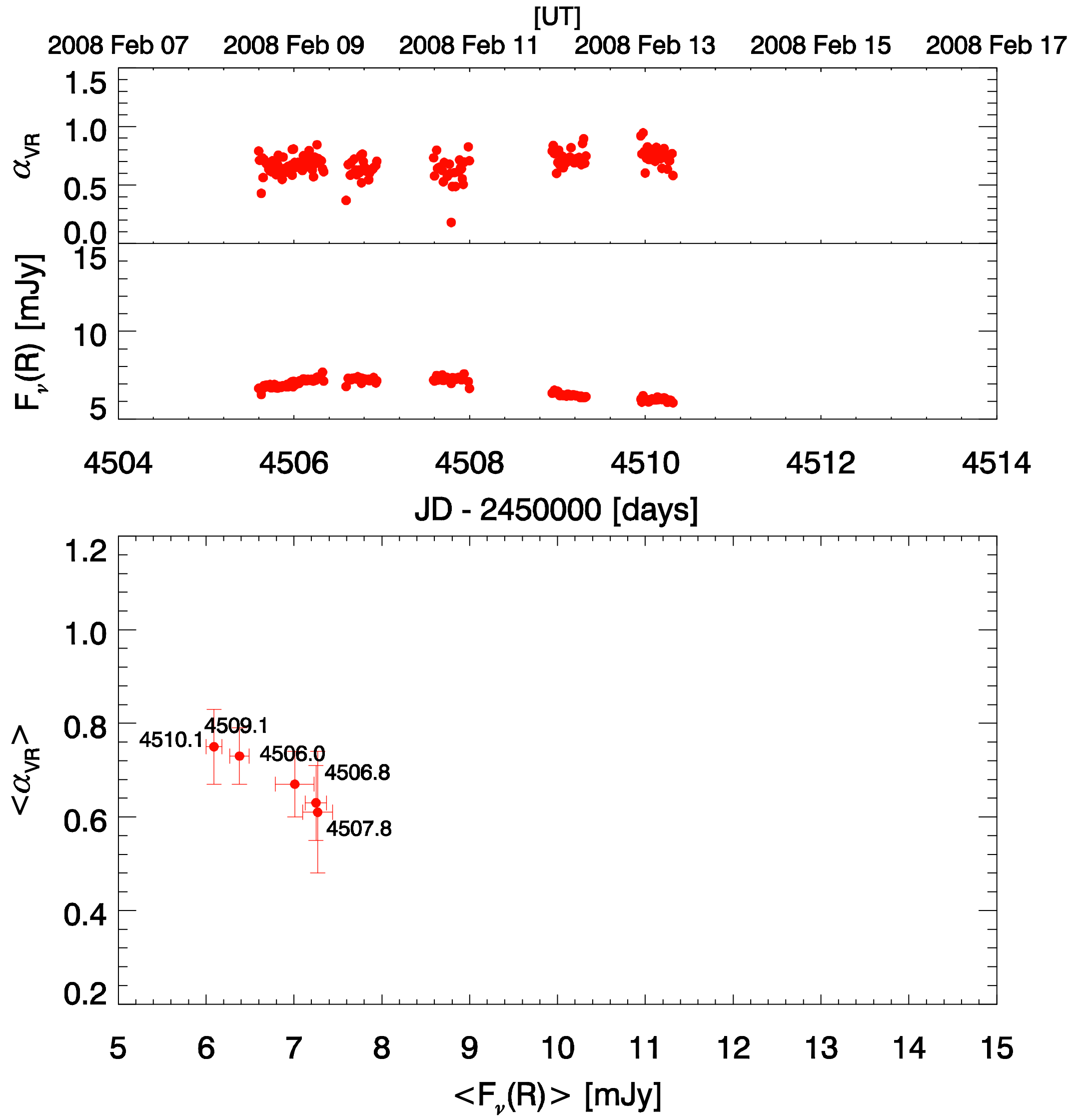

FIG. 4.11.—Same as in Figure 3.4. The data were observed from JD 2454505 to JD 24524510.

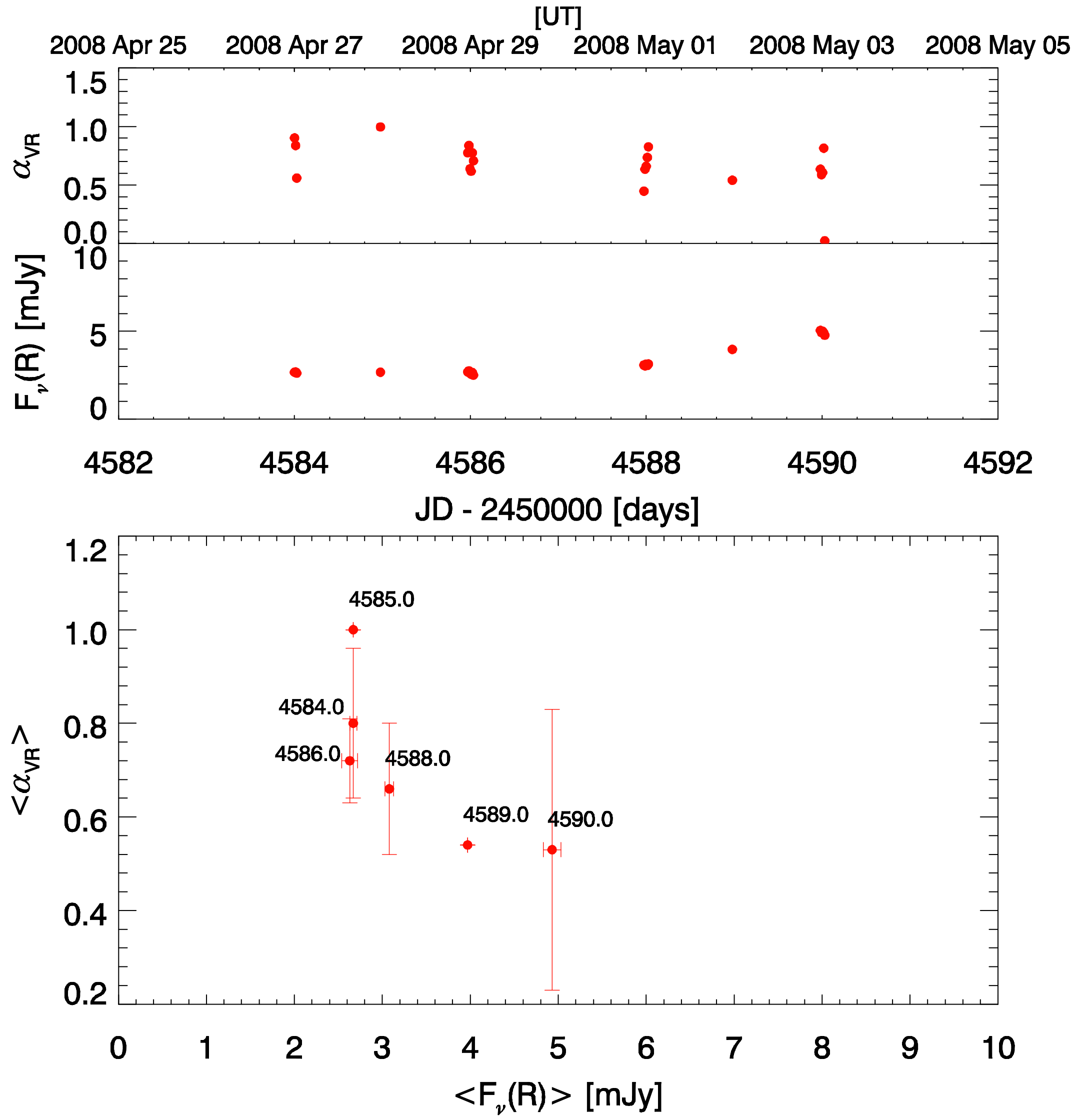

FIG. 4.12.—Same as in Figure 3.4. The data were observed from JD 2454583 to JD 24524590.

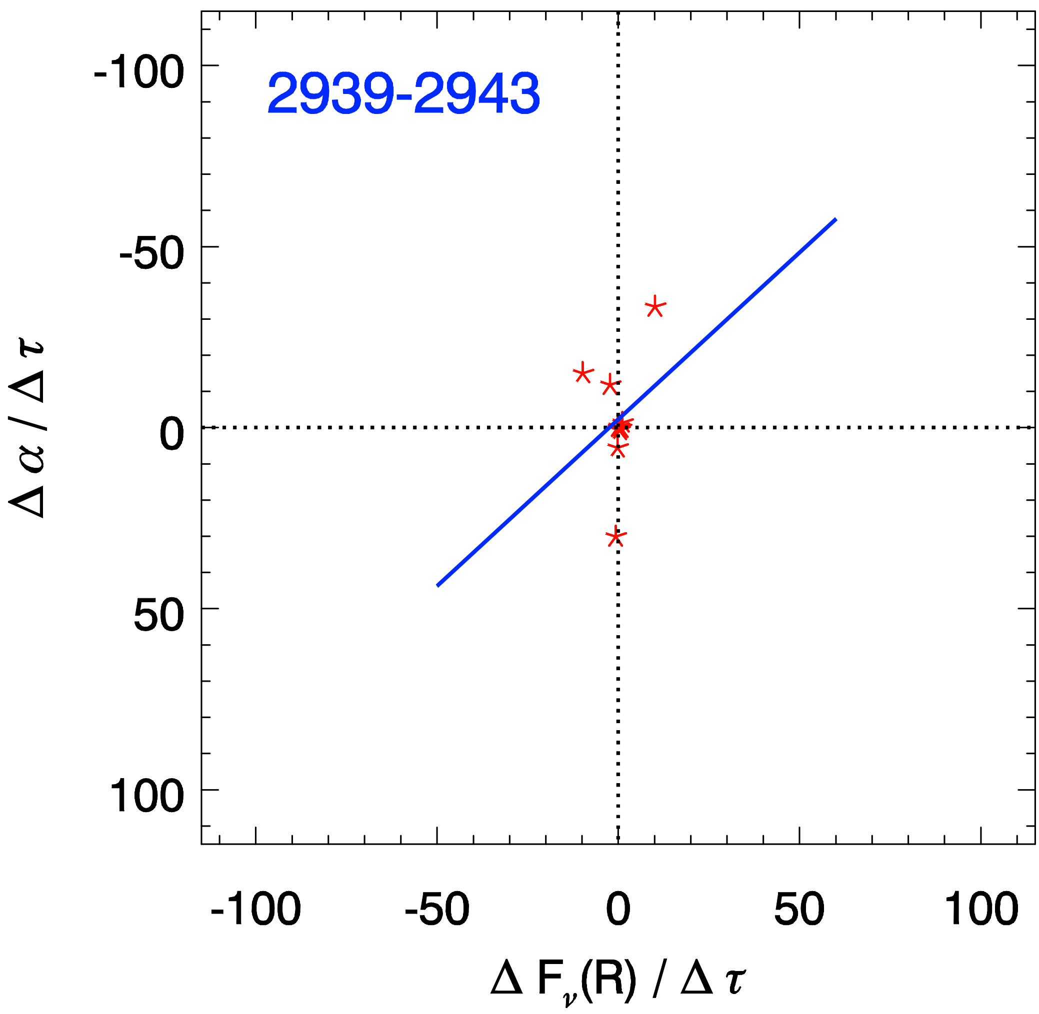

FIG. 4.13.—Variation rates of the spectral index, $\Delta\alpha_{VR}/\Delta\tau$, versus the flux density, $\Delta F_{\nu}(R)/\Delta\tau$. The data were observed from JD 2452939 to JD 2452943.

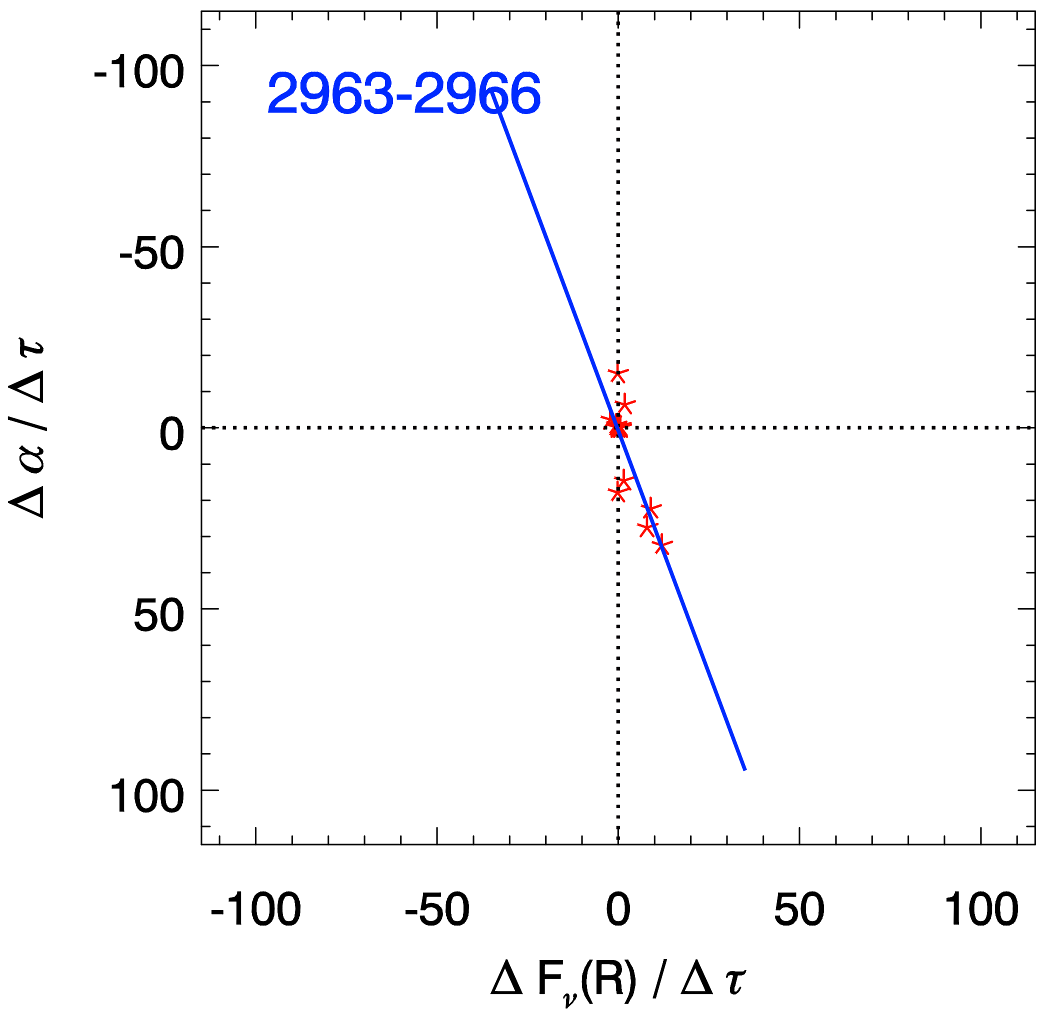

FIG. 4.14.—Same as in Figure 4.1. The data were observed from JD 2452963 to JD 2452966.

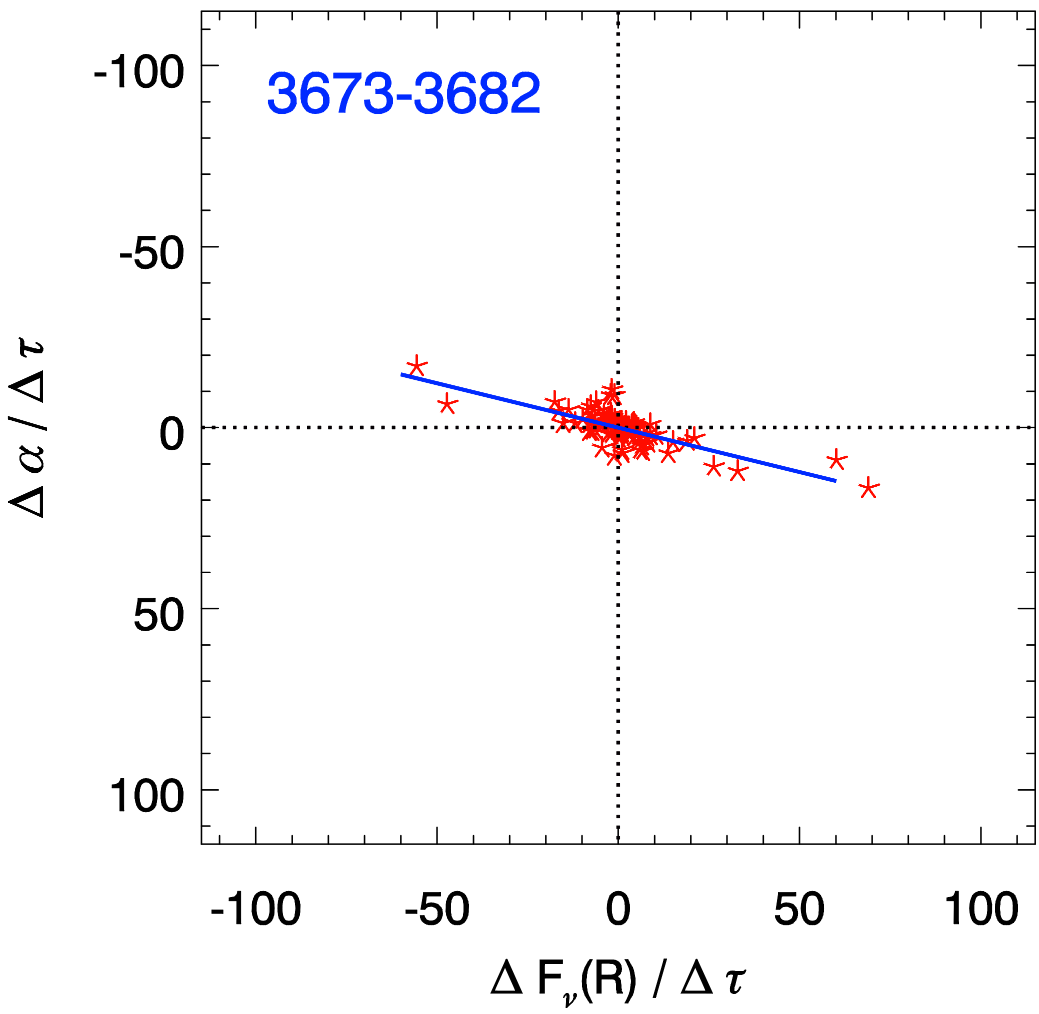

FIG. 4.15.—Same as in Figure 4.1. The data were observed from JD 2453673 to JD 2453682.

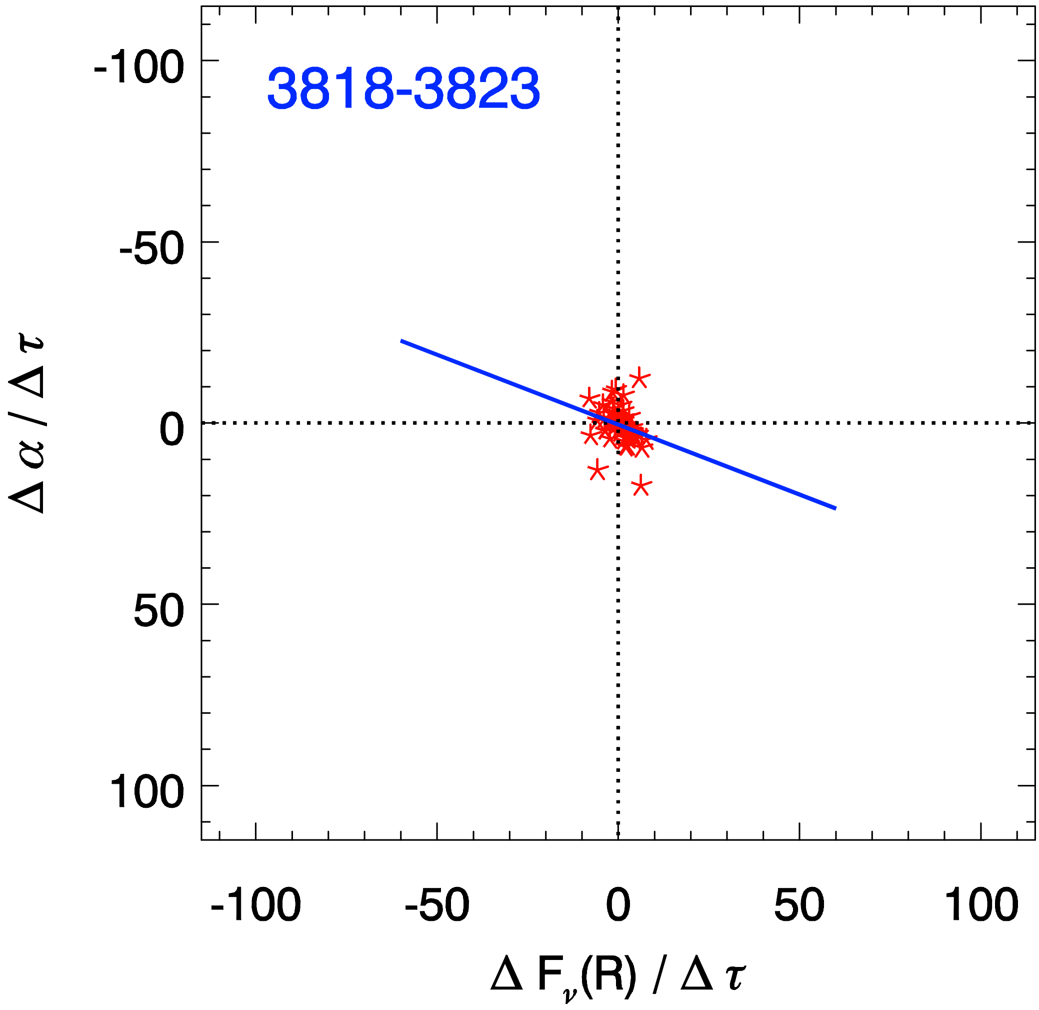

FIG. 4.16.—Same as in Figure 4.1. The data were observed from JD 2453818 to JD 2453823.

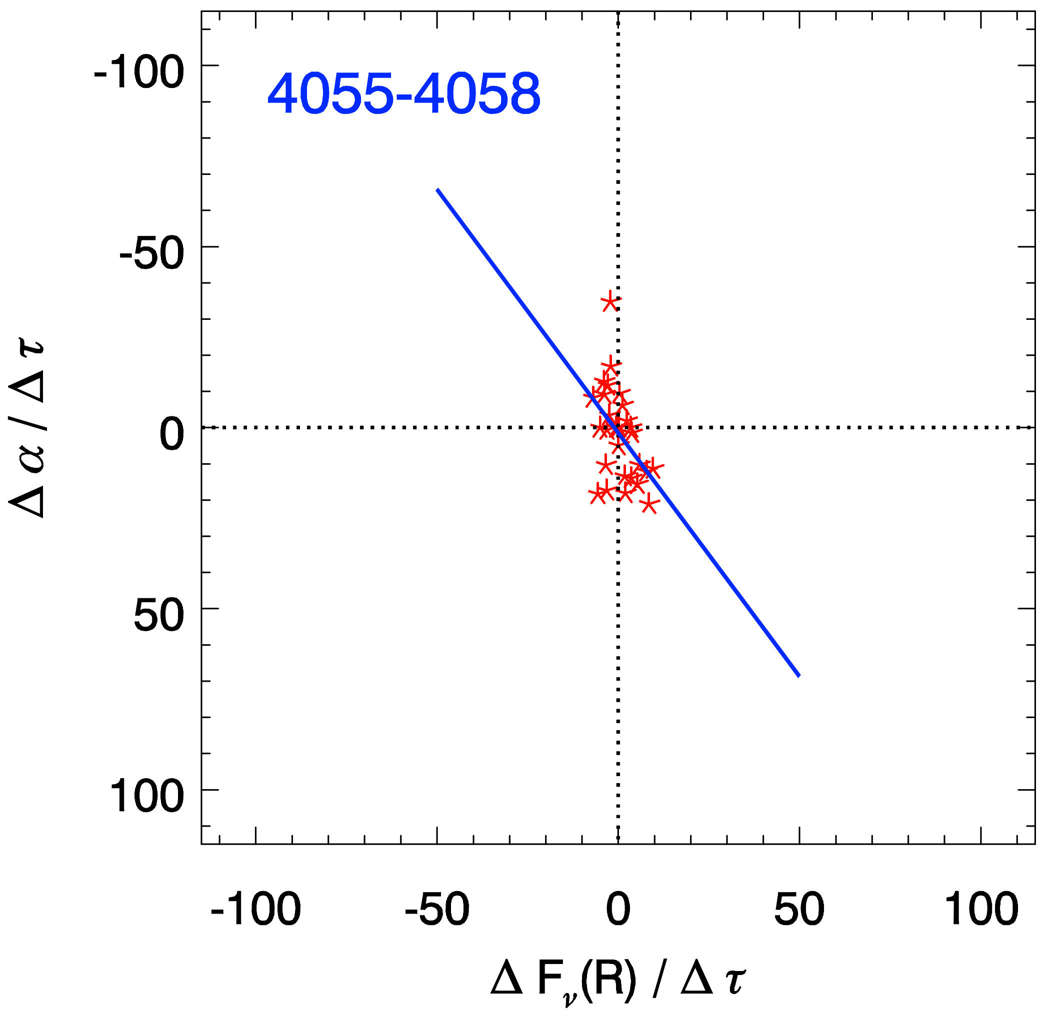

FIG. 4.17.—Same as in Figure 4.1. The data were observed from JD 2454055 to JD 2454058.

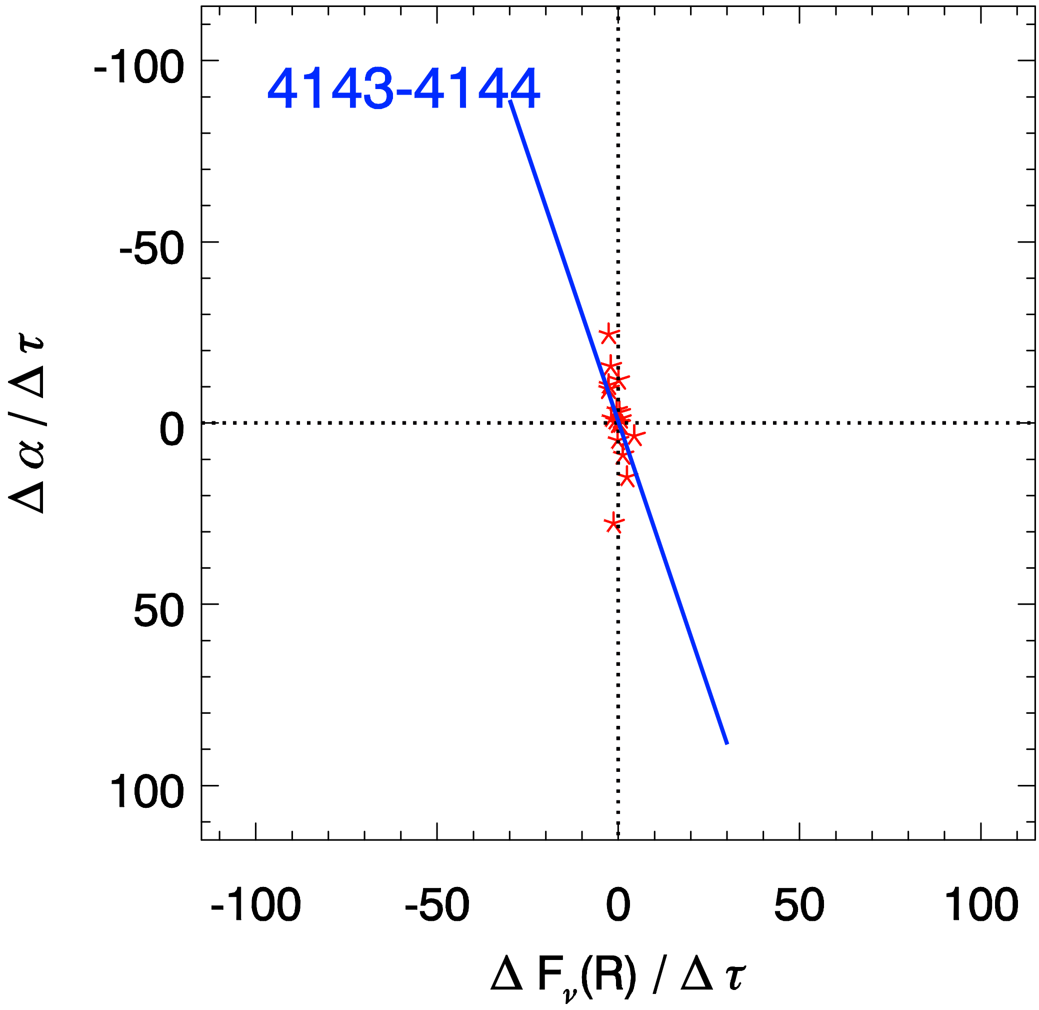

FIG. 4.18.—Same as in Figure 4.1. The data were observed from JD 2454143 to JD 2454144.

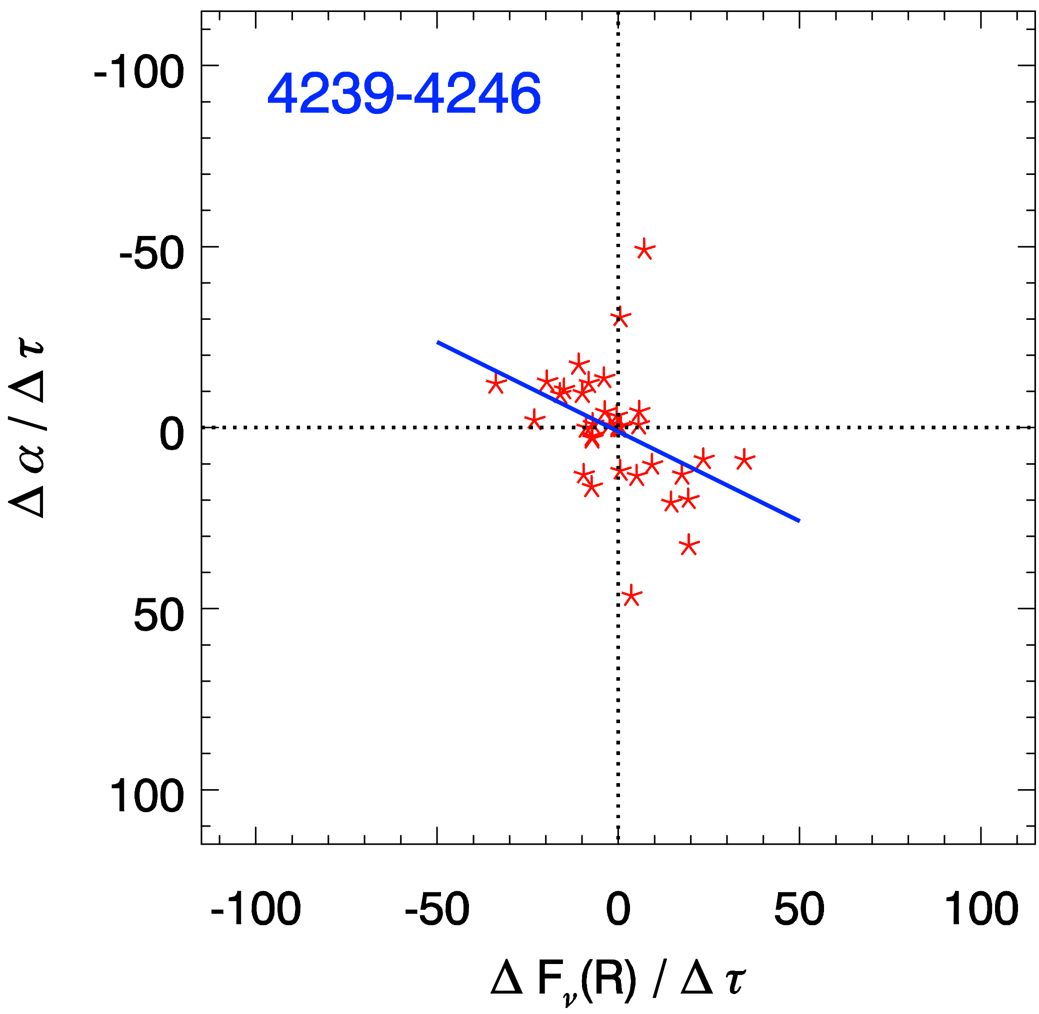

FIG. 4.19.—Same as in Figure 4.1. The data were observed from JD 2454239 to JD 2454246.

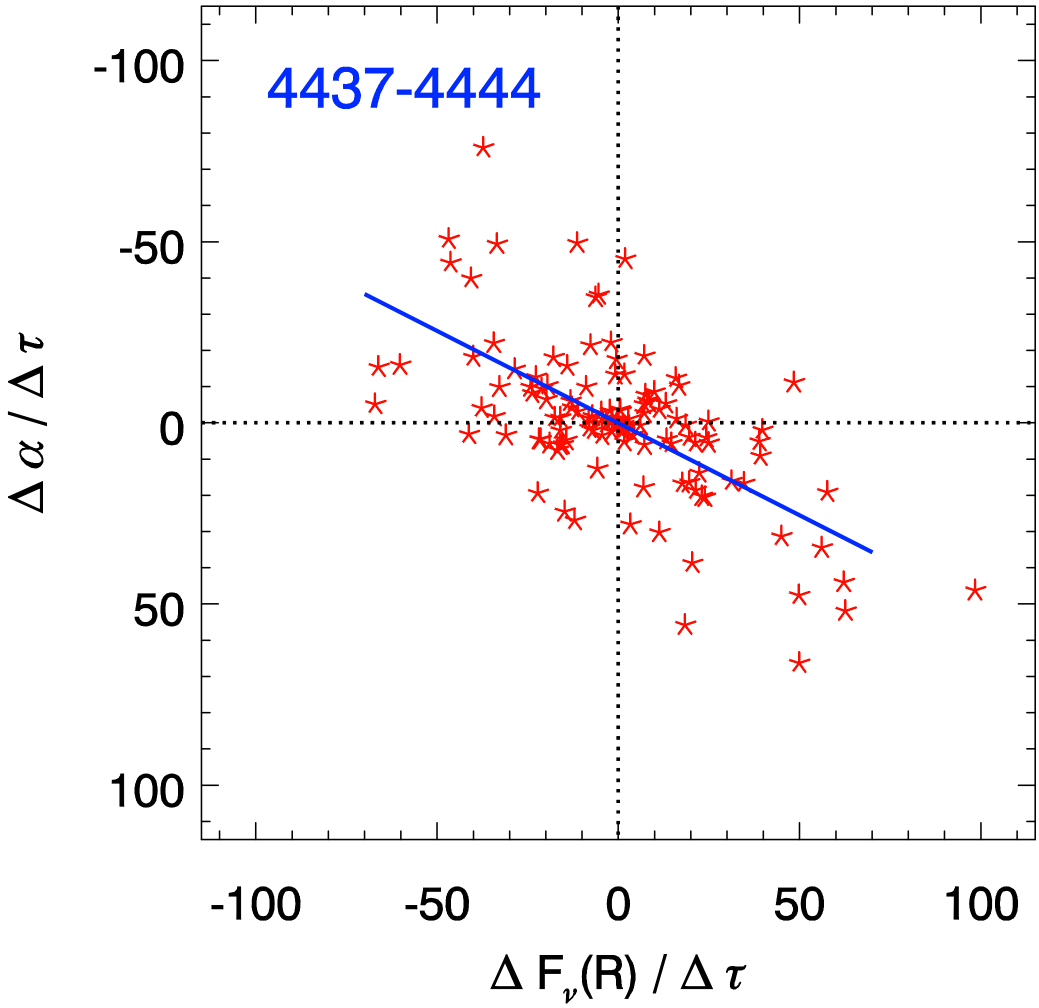

FIG. 4.20.—Same as in Figure 4.1. The data were observed from JD 2454437 to JD 2454444.

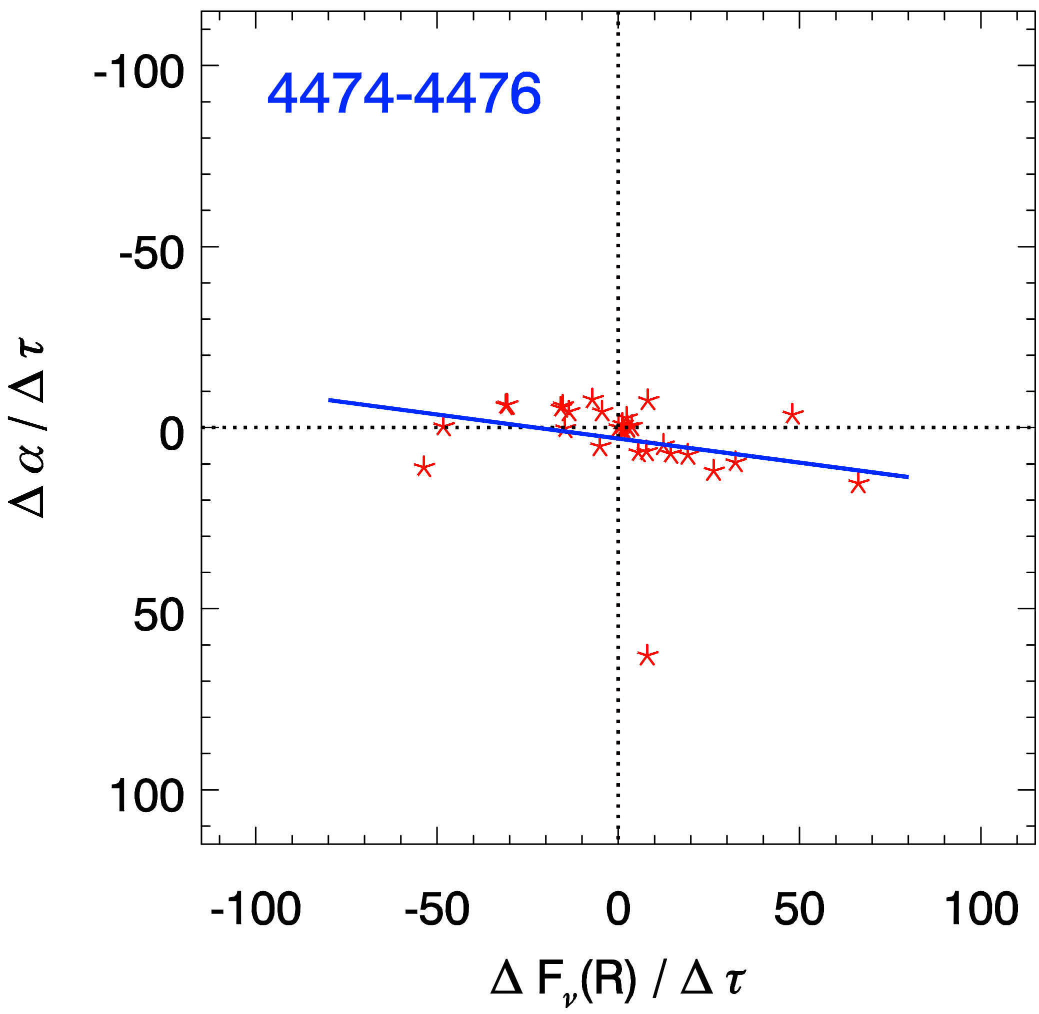

FIG. 4.21.—Same as in Figure 4.1. The data were observed from JD 2454474 to JD 2454476.

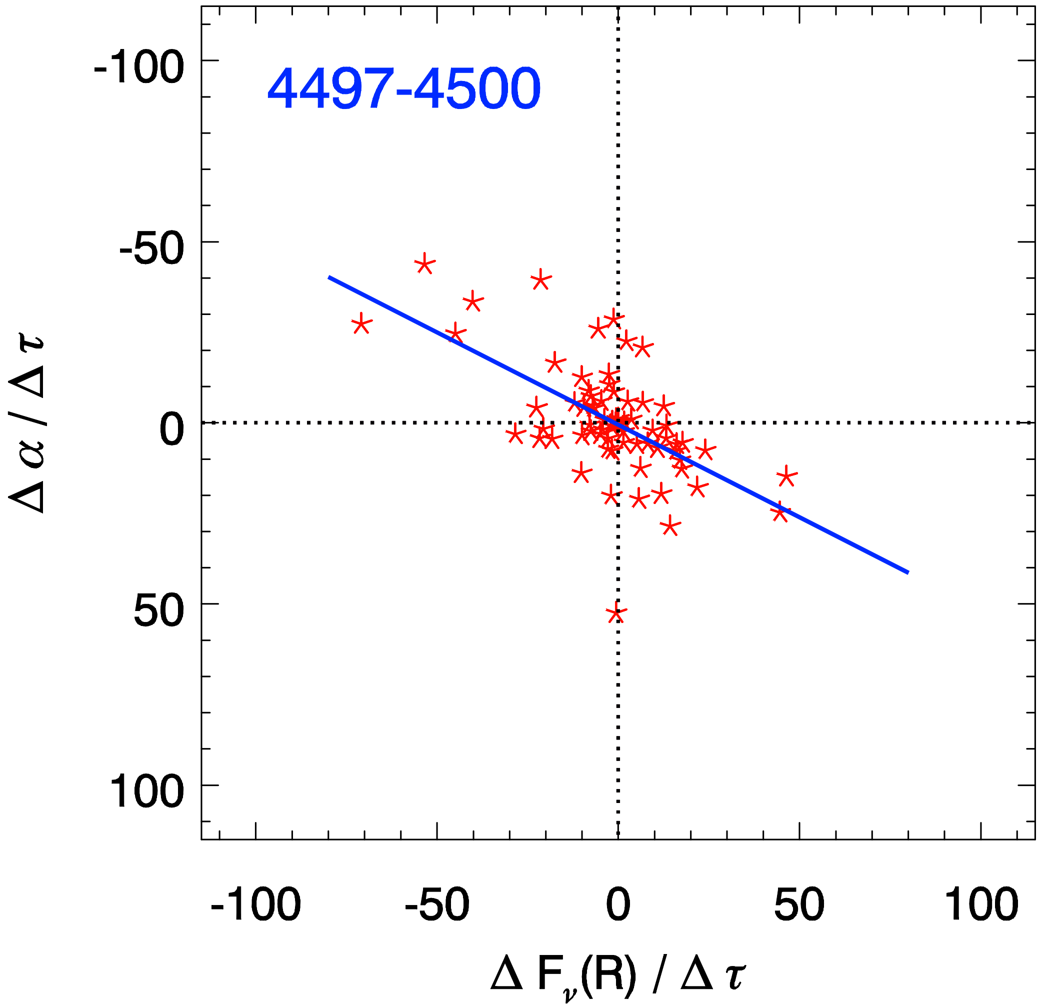

FIG. 4.22.—Same as in Figure 4.1. The data were observed from JD 2454497 to JD 2454500.

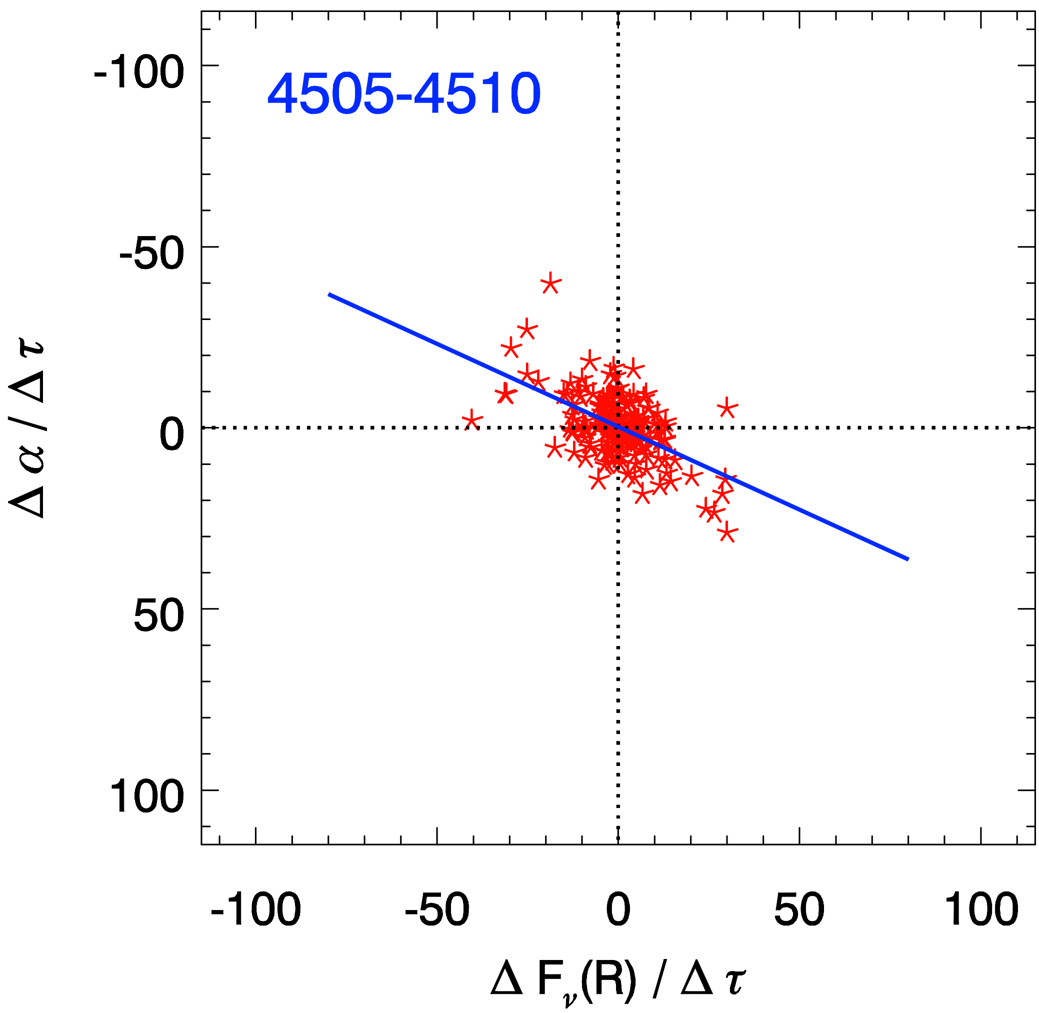

FIG. 4.23.—Same as in Figure 4.1. The data were observed from JD 2454505 to JD 2454510.

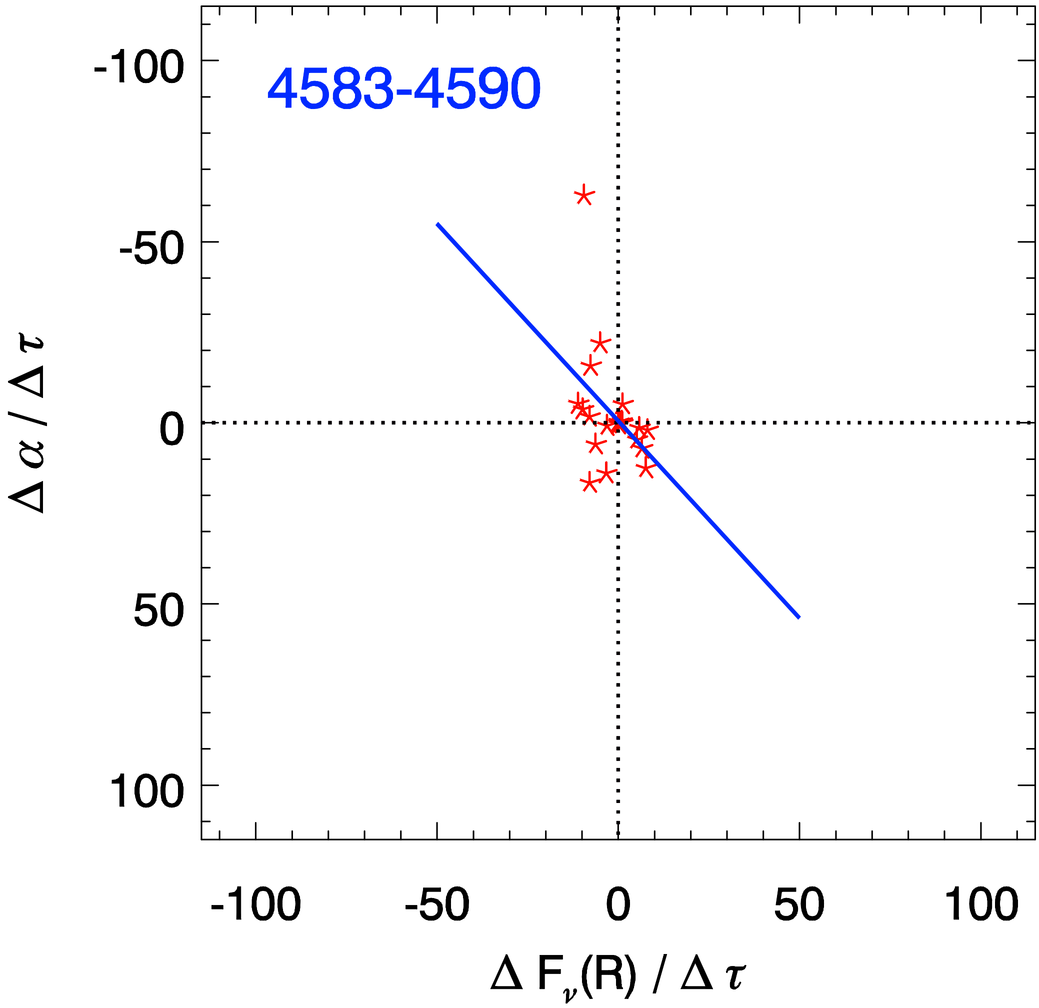

FIG. 4.24.—Same as in Figure 4.1. The data were observed from JD 2454583 to JD 2454590.

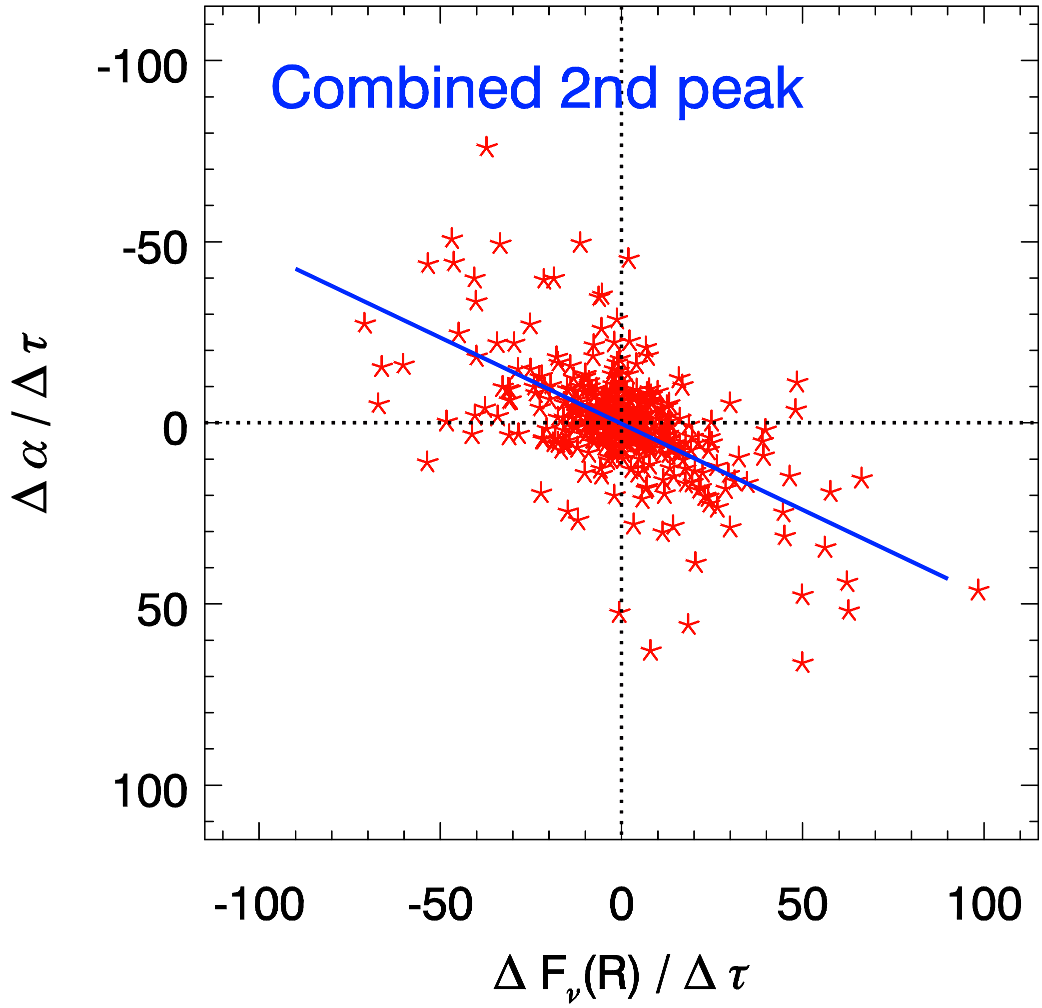

FIG. 4.25.—Same as in Figure 4.1. The data were observed during the 2nd peak.

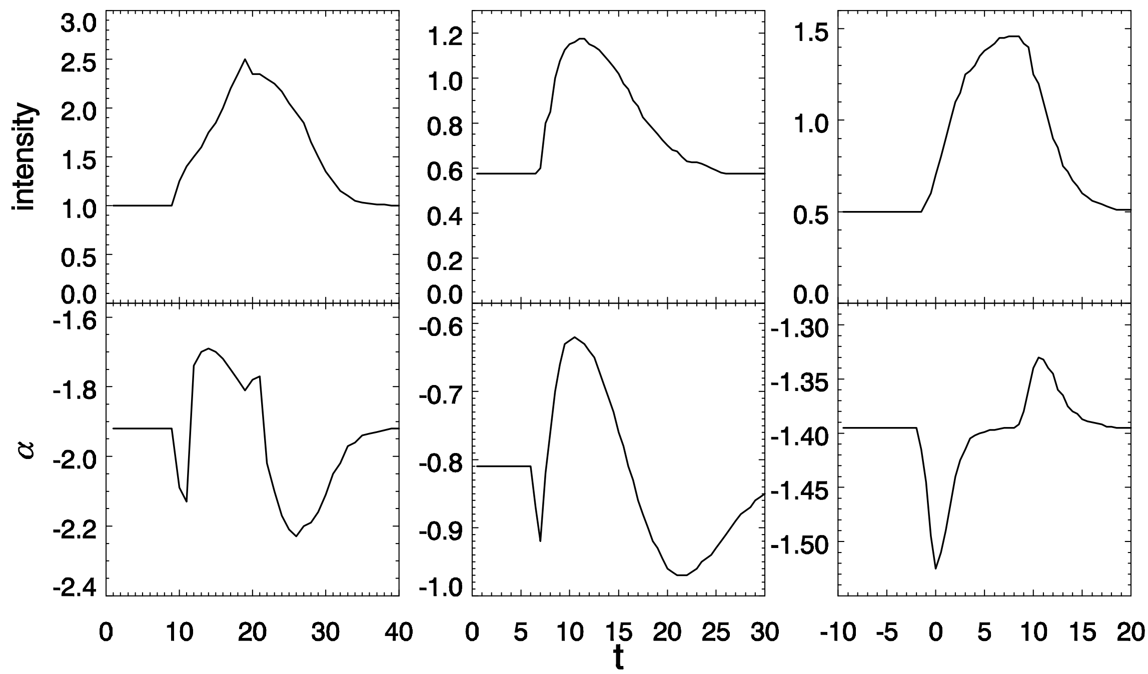

FIG. 4.26.—Light curves of the spectral index α and intensity about time for case II, case III and case IV in Kirk & Mastichiadis (1999).

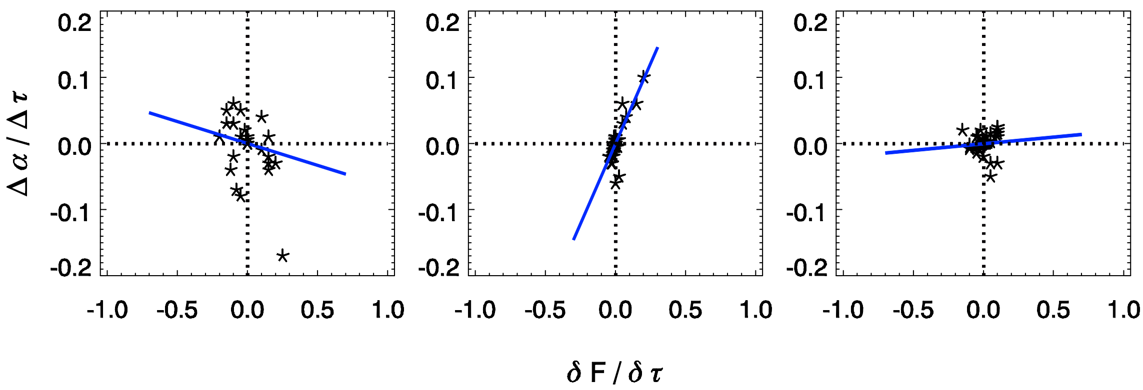

FIG. 4.27.—Variation rates of the spectral index, $\Delta\alpha/\Delta\tau$, versus the flux density, $\Delta F/\Delta\tau$ for case II, case III and case IV in Kirk & Mastichiadis (1999). The regression lines are also shown.

TABLE 4.1.—Average spectral index α_{VR} and flux density $F_\nu(R)$ per day

Date[a] (Julian Date – 2450000)	N[b]	$<F_\nu(R)>$	RMS_F	$<\sigma_{VR}>$	RMSα
2939.185	2	2.214	0.270	1.169	0.332
2941.353	2	2.457	0.006	0.738	0.253
2942.190	5	2.616	0.055	0.960	0.115
2943.028	2	3.151	0.062	0.851	0.204
2963.973	4	2.021	0.016	0.869	0.063
2965.018	3	2.633	0.002	0.973	0.132
2966.343	3	1.991	0.142	0.534	0.326
2966.990	3	1.768	0.082	0.771	0.244
3673.952	14	12.003	0.068	0.508	0.035
3676.960	12	11.353	0.303	0.494	0.064
3677.942	14	10.664	0.191	0.542	0.064
3678.948	16	12.587	0.053	0.498	0.026
3679.957	14	12.464	0.062	0.513	0.022
3680.948	15	13.606	0.065	0.502	0.041
3682.418	2	13.603	0.593	0.498	0.051
3682.913	3	13.873	0.158	0.476	0.063
3818.751	23	4.294	0.032	0.609	0.046
3819.771	18	4.462	0.058	0.593	0.048
3821.734	2	4.663	0.052	0.739	0.143
3823.729	14	4.857	0.034	0.636	0.042

TABLE 4.1.—*continued*

Date[a] (Julian Date – 2450000)	N^b	$<F_\nu(R)>$	RMS_F	$<\sigma_{VR}>$	$RMS\alpha$
4055.321	4	2.367	0.027	0.781	0.078
4057.262	12	2.587	0.082	0.629	0.232
4058.284	15	2.473	0.036	0.757	0.114
4143.090	4	1.740	0.020	0.809	0.171
4144.180	14	1.844	0.034	0.713	0.135
4239.687	8	5.848	0.104	0.548	0.195
4240.688	8	5.563	0.101	0.572	0.078
4241.684	7	5.626	0.135	0.557	0.126
4244.714	2	5.698	0.504	0.730	0.181
4245.684	7	5.909	0.093	0.579	0.141
4246.665	6	5.662	0.067	0.554	0.090
4437.926	15	9.704	0.135	0.773	0.074
4438.995	25	9.455	0.197	0.722	0.112
4440.028	34	10.323	0.331	0.749	0.119
4440.939	17	10.305	0.156	0.681	0.102
4443.274	18	9.317	0.392	0.758	0.222
4444.268	19	8.550	0.440	0.762	0.378
4474.827	4	10.512	0.324	0.576	0.135
4475.898	26	12.842	0.286	0.571	0.135
4497.969	15	8.562	0.181	0.698	0.092
4498.812	32	7.997	0.424	0.664	0.193
4499.866	26	7.274	0.106	0.654	0.130

TABLE 4.1.—*continued*

Date[a] (Julian Date – 2450000)	N[b]	$<F_{\nu}(R)>$[c]	RMS_F[d]	$<\sigma_{VR}>$[e]	$RMS\alpha$[d]
4505.957	65	7.012	0.224	0.673	0.068
4506.765	25	7.246	0.119	0.630	0.080
4507.795	24	7.271	0.167	0.615	0.128
4509.130	29	6.378	0.114	0.734	0.064
4510.132	30	6.092	0.091	0.752	0.078
4584.009	4	2.666	0.037	0.797	0.161
4584.979	1	2.667	0.000	0.996	0.000
4586.003	6	2.633	0.090	0.725	0.086
4588.000	5	3.083	0.047	0.661	0.141
4588.980	1	3.970	0.000	0.541	0.000
4590.005	5	4.930	0.104	0.533	0.300

[a] Average date during the day.

[b] Number of data points during the day

[c] Average Flux during the day

[d] Root–mean–square of the data during the day.

[e] Average spectral index during the day

TABLE 4.2.—Variation rates of the spectral index, $\Delta\alpha_{VR}/\Delta\tau$, versus the flux density, $\Delta F_{\nu}(R)/\Delta\tau$ from 2003 September to 2008 May. We grouped the data based on the continuity of nights, and marked with the Julian Date (–2450000) of the beginning night in the group.

Date (Julian Date – 2450000)	N	Slope	R	Probs.
2939-2943	11	-0.91	-0.27	0.42
2963-2966	13	2.76	0.82	0.00
3673-3682[a]	90	0.24	0.76	0.00
3818-3823	57	0.40	0.27	0.00
4055-4058	31	1.37	0.46	0.01
4143-4144	18	2.99	0.47	0.05
4239-4246	37	0.49	0.39	0.01
4437-4444[b]	128	0.51	0.68	0.00
4474-4476[b]	30	0.14	0.25	0.18
4497-4500[b]	73	0.51	0.79	0.00
4505-4510[b]	173	0.46	0.55	0.00
4583-4590	22	1.11	0.41	0.06
4437-4510[c]	404	0.50	0.67	0.00

[a] Data during the first peak.

[b] Data during the second peak.

[c] Combined data during the second peak.

TABLE 4.3.—Variation rates of the spectral index, $\Delta\alpha/\Delta\tau$, versus the flux density, $\Delta F/\Delta\tau$ for case II, case III and case IV in Kirk & Mastichiadis (1999)

Case	Slope	N	R	Probs.
II($t_{cool} >> t_{var} >> t_{acc}$)	-0.07	40	-0.08	0.61
III ($t_{cool} >> t_{acc} >> t_{var}$)	0.49	60	0.80	0.00
IV ($t_{cool} \approx t_{acc} \approx t_{var}$)	60	0.00	0.08	0.52

Chapter 5

Summary

We present the result of optical monitoring of the blazer OJ 287 from 2003 September to 2008 May. The main results can be summarized as follows:

1. During the monitoring campaign, the target shows strong flux variations of ΔB = 1.37 mag (14.20–15.57 mag), ΔV = 2.68 mag (13.71–16.39 mag), ΔR = 2.31 mag (13.30–15.61 mag), and ΔI = 2.19 mag (12.71–14.90 mag).
2. The spectral index values in 2003–2008 varies from –0.4 to 1.5. We can notice the significant variabilities of the spectral index during the flares. On the other hand, the long-term spectral variability in our data seems achromatic.
3. The correlation between the spectral index and the flux of the blazar OJ 287 in optical band. correlation implies that the spectrum becomes bluer (flatter) when the source is brighter. And this result is in accord with the common color change

tendency in blazars.

4. In order to analyse the variation correlations of the flux and the spectral index, we introduce a method to compare the variation rates of the two parameters.
5. By comparing our results with the particle acceleration model of Kirk & Mastichiadis (1999), we suggest the possible emission mechanisms during the outburst.

Bibliography

Abraham, Z. 2000, A&A, 355, 915

Arimoto, J., Sadakane, K., Honda, S., & Tanabe, K. 1997, PASP, 109, 300

Blandford, R. D., & Rees, M. J. 1978, in Pittsburgh Conference on BL Lac Objects, Pittsburgh, PA, April 24-26, 1978, ed. A. M. Wolfe (Univ. of Pittsburgh Press), 328

Böttcher, M., & Chiang, J. 2002, ApJ, 581, 127

Chiang, J., & Böttcher, M. 2002, ApJ, 564, 92

Ciprini, S., Tosti, G., Teräsranta, H., & Aller, H. D. 2004, MNRAS, 348, 1379

Ciprini, S., et al. 2007, A&A, 467, 465

Clements, S. D., & Carini, M. T. 2001, AJ, 121, 90

Cox, A. N. 2000, Allen's Astrophysical Quantities(Berlin: Springer)

D' Amicis, R., Nesci, R., Massaro, E., Maesano, M., Montagni, F., & D' Alessio, F. 2002, PASA, 19, 111

De Diego, J. A., Kidger, M. R., Gonzáles-Pérez, J. N., & Lehto, H. J. 1997, A&A, 318, 331

Falomo, R., Bersanelli, M., Bouchet, P., Tanzi, E. G. 1993, AJ, 106, 11

Fan, J. H., et al. 1998, A&AS, 133, 163

Fan, J. H., Xie, G. Z., Pecontal, E., Pecontal, A., & Copin, Y. 1998b, ApJ, 507, 173

Fan, J. H., Zhang, Y. W., Qian, B. C., Tao, J., Liu, Y., & Hua, T. X. 2009, ApJS, 181, 466

Fiorucci, M., Ciprini, S., & Tosti G. 2004, A&A, 419, 25

Gear, W. K., Robson, E. I., & Brown, L. M. J. 1986, Nature, 1986, 324, 11

Georganopoulos, M., & Marscher, A. P. 1998, ApJ, 506, L11

Ghisellini, G., et al. 1997, A&A, 327, 61

Giommi P., et al. 1999, A&A, 351, 59

González-Pérez, J. N., Kidger, M. R., & Martín-Luis, F. 2001, AJ, 122, 2055

Gu, M. F., Lee C. -U., Pak, S., Yim, H. S., & Fletcher A. B. 2006, A&A, 450, 39

Gupta, A. C., & Joshi, U. C. 2005, A&A, 440, 855

Hughes, P. A., Aller, H. D., & Aller, M. F. 1998, ApJ, 503, 662

Igumenshchev, I. V., & Abramowicz, M. A. 1999, MNRAS, 303, 309

Ivanov, P. B., Igumenshchev, I. V., & Novikov, I. D. 1998, ApJ, 507, 131

Jia, G. B., Cen, X. F., Ma, H. Y., & Wang, J. C. 1998, A&AS, 129, 569

Katajainen, S., et al. 2000, A&AS, 143, 357

Kataoka, J., et al. 2000, ApJ, 528, 243

Katz, J. I. 1997, ApJ, 478, 527

Kidger, M. R., et al. 1995, A&AS, 113, 431

Kirk, J. G., Rieger, F. M., & Mastichiadis, A. 1998, A&A, 333, 452

Kirk, J. G., & Mastichiadis, A. 1999, Astropart. Phys., 11, 45

Lee, C. -U., Park, S. S., Kim, C. H., & Byun, Y. I. 2003, JASS, 20, 143

Lehto, H. J., & Valtonen, M. J. 1996, ApJ, 460, 207

Maesano, M., Montagni, F., Massaro, E., & Nesci, R. 1997, A&AS, 122, 267

Massaro, E., et al. 1996, A&A, 314, 87

Massaro, F., Giommi, P., Tosti, G., Cassetti, A., Nesci, R., Perri, M., Burrows, D., & Gerehls, N. 2008, A&A, 489, 1047

Mastichiadis, A., & Kirk, J. G. 2002, PASA, 19, 138

Moles, M., García-Pelayo, J. M., Masegosa, J., & Aparicio, A. 1985, ApJS, 58, 255

Padovani, P., & Giommi, P. 1995, MNRAS, 277, 1477

Papadakis, I. E., Villata, M., & Raiteri, C. M. 2007, A&A, 470, 857

Pian, E., Falomo, R., Scarpa, R., & Treves, A. 1994, ApJ, 432, 547

Pursimo, T., et al. 2000, A&AS, 146, 141

Raiteri, C. M., Villata, M., Takalo, L. O. 1999, OJ-94 Annual meeting 1999, Blazar Monitoring towards the Third Millenium, Osservatorio Astronomico di Torino, Pino Torinese

Raiteri, C. M. et al. 2008, A&A, 491, 755

Ravasio, M., Tagliaferri, G., Ghisellini, G., & Tavecchio, F. 2004, A&A, 424, 841

Scarpa, R., Urry, C. M., Falomo, R., Pesce, J. E., & Treves, A. 2000, ApJ, 532, 740

Sembay, S. et al. 1993, ApJ, 404, 112

Sillanpää, A., Haarala, S., Valtonen, M. J., Sundelius, B., & Byrd, G. G. 1988a, ApJ, 325, 628

Sillanpää, A., Haarala, S., & Korhonen, T. 1988b, A&AS, 72, 347

Sillanpää, A., et al. 1996a, A&A, 305, L17

Sillanpää, A., et al. 1996b, A&A, 315, L13

Stalin, C. S., Gopal-Krishna, Sagar, R., Wiita, P. J., Mohan, V., & Pandey, A. K. 2006, MNRAS, 366, 1337

Sundelius, B., Wahde, M., Lehto, H. J., & Valtonen, M. J. 1996, in Blazar Continuum Variability, ed. H. R. Miller et al., APS Conf. Ser., 110, 99

Sundelius, B., Wahde, M., Lehto, H. J., & Valtonen, M. J. 1997, ApJ, 484, 180

Takalo, L. O., Sillanpää, A. 1989, A&A, 218, 45

Takalo, L. O., et al. 1996, A&AS, 120, 313

Tosti, G. 1998, A&AS, 130, 109

Vagnetti, F., Trevese, D., & Nesci, R. 2003, ApJ, 590, 123

Valtaoja, E., Teräsranta, H., Tornikoski, M., Sillanpää, A., Aller, M. F., Aller, H. D., & Hughes, P. A. 2000, ApJ, 531, 744

Valtonen, M. J., Lehto, H. J. 1997, ApJ, 481, L5

Valtonen, M. J. 2007, ApJ, 659, 1074

Valtonen, M., Kidger, M., Lehto, H., & Poyner, G. 2008a, A&A, 477, 407

Valtonen, M. J., et al. 2008b, Nature, 452, 17

Valtonen, M. J., et al. 2009, ApJ, 698, 781

Villata, M., Raiteri, C. M., Sillanpää, A., & Takalo, L. O. 1998, MNRAS, 293, L13

Ulrich, M. -H., Maraschi, L., & Urry, C. M. 1997, ARA&A, 35, 445

Urry, C. M., & Padovani, P. 1995, PASP, 107, 803

Urry, C. M., Scarpa, R., O'Dowd, M., Falomo, R., Pesce, J. E., & Treves, A. 2000, ApJ, 532, 816

Zheng, Y. G., Zhang, X., & Bi, X. W. 2007, PASP, 119, 477

Zheng, Y. G., Zhang, X., Bi, X. W., Hao, J. M., & Zhang, H. J. 2008, MNRAS, 385, 823

Abstract (Korean)

본 연구에서는 지난 2003년 9월부터 2008년 5월까지의 기간 동안 소백산 천문대의 0.6m 광학 망원경과 1.0m 무인 광학 망원경의 $BVRI$ 필터를 사용하여 blazar OJ 287을 광학 관측하여 얻어진 결과를 토대로 분석 및 토의 하였다. 이와 같은 캠페인을 하는 동안에 OJ 287은 ΔB = 1.37 등급 (14.20 −15.57 등급), ΔV=2.68 등급 (13.71−16.39 등급), ΔR = 2.31 등급 (13.30−15.61 등급), 그리고 ΔI = 2.19 등급 (12.71−14.90 등급)의 변화를 보였다. 또한 관측하는 동안에 색의 변화도 보여졌다. 우리는 플럭스와 스펙트럼 지수 사이의 변화 관계를 분석하기 위해 두 변수의 시간에 따른 변화율을 비교해 보는 방법을 제안하였다. Kirk & Mastichiadis (1999)의 입자 가속 모델과 우리 결과를 비교해 봄으로써, 우리는 blazer OJ 287이 Outburst 하는 동안에 설명 할 수 있는 방출 메커니즘을 제안한다.

Acknowledgement (Korean)

지난 2년 동안 석사과정을 마치면서 고마웠던 모든 분들께 감사의 인사를 드립니다. 많은 분들의 따뜻한 배려와 격려가 있었기에 논문을 무사히 마칠 수 있었습니다.

처음 연구실을 들어갔던 학부시절부터 대학원 석사과정 동안 학문의 길을 걸을 수 있도록 항상 꼼꼼함, 성실함과 자상함으로 지도해주신 존경하는 박수종 교수님께 가장 감사의 말을 전하고 싶습니다. 교수님을 통하여 연구의 많은 부분뿐만 아니라 삶에 대하여 많은 부분을 배울 수 있었습니다. 교수님과 함께 연구할 수 있었던 것은 저에게 커다란 행운이었습니다.

또한 본 주제로 논문을 쓸 수 있도록 함께 해주신 blazar 관측 팀, 이충욱 박사님, 임홍서 박사님 그리고 학위논문을 심사해 주신 손봉원 박사님께 감사의 말을 전합니다. 특히 관측 데이터 처리에 대해 많은 시간을 내어 친절하게 가르쳐 주셨던 이충욱 박사님께 다시 한번 감사 드립니다.

그리고 연구에 관하여 항상 격려해주시며 따뜻하게 조언해주시던 송인옥 박사님과, 논문에 관해서 많은 조언을 아끼지 않으셨던 박원기 박사님께 더불어 고마운 마음을 표합니다.

언제나 인자한 모습으로 다가와 주신 김갑성 교수님, 학자로서의 모범을 보여주신 김상준 교수님, 학위 논문을 심사해 주신 장민환 교수님, 신앙과 삶에 관하여 모범이 되어 주신 문용재 교수님 그리고 여러 가지 조언과 가르침을 주셨던 김성수 교수님, 최광선 교수님, 이동훈 교수님께 감사 드립니다.

적외선 실험실 동료들, 적외선 실험실이 처음 생겼을 때부터 함께 했던 정미언니와 상혁이, 그리고 항상 세심하게 배려해 주던 희영이, 모르는

부분들을 친절하게 가르쳐주던 용석 오빠, 함께 기도하던 은빈 언니, 착한 재영이 그리고 열심히 공부하는 Huynh Anh과 웃음을 선사하던 배성이에게 고맙다는 말을 전합니다. 또한 잠시 동안 이었지만 연구실에서 함께 했던 대욱 오빠와 진규 오빠에게도 고마움을 표합니다. 그리고 우주공간물리 연구실, 천체물리 연구실, 태양물리 연구실, 행성 연구실, 우주기상 연구실, 태양권 플라즈마 연구실에서 함께 공부했던 선배님들과 후배들을 비롯한 많은 분들이 저에게 큰 힘이 되었습니다.

대학원 입학 전부터 함께 진로에 관해 고민하고 나누던 진혜, 고민이 있을 때마다 상담을 해주고 도움을 주었던 새품 언니와 승현 선배, 그리고 애란이와 03학번 친구들에게 고마움을 전합니다. 또한 천문학을 계속 할 수 있도록 항상 용기를 주었던 선화언니에게 고맙다는 말을 전하고 싶습니다.

내가 흔들릴 때마다 따끔한 충고를 아끼지 않았던 경민이, 대학 시절 함께 많은 시간을 보낸 수현이, 가장 오랫동안 알아온 초등학교 친구 은영이, 중학교 때부터 함께 해오며 나를 가장 잘 알고 힘들 때 마음으로 함께 울어주던 소중한 친구 소현이와 아현이, 은선이 그리고 만나면 항상 따뜻하게 맞아주던 소연언니와 미경이에게 고마움을 전합니다.

이 밖에도 여기에 다 적지 못하였지만 이 논문을 쓰면서 많은 도움을 주시고 저에게 힘을 주셨던 모든 분들께 감사 드립니다.

마지막으로 부족한 누나를 잘 따라주는 착한 내 동생 재웅이와, 함께 하는 것 만으로도 내게 너무 큰 힘이 되어 주며, 나를 끝까지 믿어주시며 격려해주시는 나의 가장 큰 버팀목이자 내가 가장 사랑하고 존경하는 아버지와 어머니 그리고 하나님께 이 논문을 바칩니다.